LETTER

doi:10.1038/nature14986

A marine biogenic source of atmospheric ice-nucleating particles

Theodore W. Wilson[1]*, Luis A. Ladino[2]*, Peter A. Alpert[3], Mark N. Breckels[4], Ian M. Brooks[1], Jo Browse[1], Susannah M. Burrows[5], Kenneth S. Carslaw[1], J. Alex Huffman[6], Christopher Judd[1], Wendy P. Kilthau[7], Ryan H. Mason[8], Gordon McFiggans[9], Lisa A. Miller[10], Juan J. Nájera[9], Elena Polishchuk[8], Stuart Rae[9], Corinne L. Schiller[11], Meng Si[8], Jesús Vergara Temprado[1], Thomas F. Whale[1], Jenny P. S. Wong[2], Oliver Wurl[12]†, Jacqueline D. Yakobi-Hancock[2], Jonathan P. D. Abbatt[2], Josephine Y. Aller[7], Allan K. Bertram[8], Daniel A. Knopf[3] & Benjamin J. Murray[1]

The amount of ice present in clouds can affect cloud lifetime, precipitation and radiative properties[1,2]. The formation of ice in clouds is facilitated by the presence of airborne ice-nucleating particles[1,2]. Sea spray is one of the major global sources of atmospheric particles, but it is unclear to what extent these particles are capable of nucleating ice[3–11]. Sea-spray aerosol contains large amounts of organic material that is ejected into the atmosphere during bubble bursting at the organically enriched sea–air interface or sea surface microlayer[12–19]. Here we show that organic material in the sea surface microlayer nucleates ice under conditions relevant for mixed-phase cloud and high-altitude ice cloud formation. The ice-nucleating material is probably biogenic and less than approximately 0.2 micrometres in size. We find that exudates separated from cells of the marine diatom *Thalassiosira pseudonana* nucleate ice, and propose that organic material associated with phytoplankton cell exudates is a likely candidate for the observed ice-nucleating ability of the microlayer samples. Global model simulations of marine organic aerosol, in combination with our measurements, suggest that marine organic material may be an important source of ice-nucleating particles in remote marine environments such as the Southern Ocean, North Pacific Ocean and North Atlantic Ocean.

Atmospheric ice-nucleating particles (INPs) allow ice to nucleate heterogeneously at higher temperatures or lower relative humidity than is typical for homogeneous ice nucleation. Heterogeneous ice nucleation proceeds via different pathways depending on temperature and humidity. In low-altitude mixed-phase clouds, INPs are commonly immersed in supercooled liquid droplets and freezing can occur on them at temperatures between −36 °C and 0 °C (ref. 2). At higher altitudes and lower temperatures (less than −36 °C, the conditions under which cirrus clouds form), nucleation occurs below water saturation, proceeding by homogeneous, deposition or immersion-in-solution nucleation[1]. Understanding the sources of atmospheric INPs is important because they affect cloud lifetime, cloud albedo and precipitation[1,2]. Recent modelling work has shown that the ocean is potentially an important source of biogenic atmospheric INPs, particularly in remote, high-latitude regions[9,10]. However, it has never been directly shown that there is a source of atmospheric INPs associated with organic material found in marine waters or sea-spray aerosol.

Organic material makes up a substantial fraction of submicrometre sea-spray aerosol and it is estimated that $10 \pm 5\,\mathrm{Tg\,yr^{-1}}$ of primary organic submicrometre aerosol is emitted from marine sources globally[12]. Rising bubbles scavenge surface active organic material from the water column at their interfaces and this process facilitates the formation of the organic enriched sea–air interface known as the sea surface microlayer (SML). This organic material is ejected into the atmosphere during bubble bursting, resulting in sea-spray aerosol

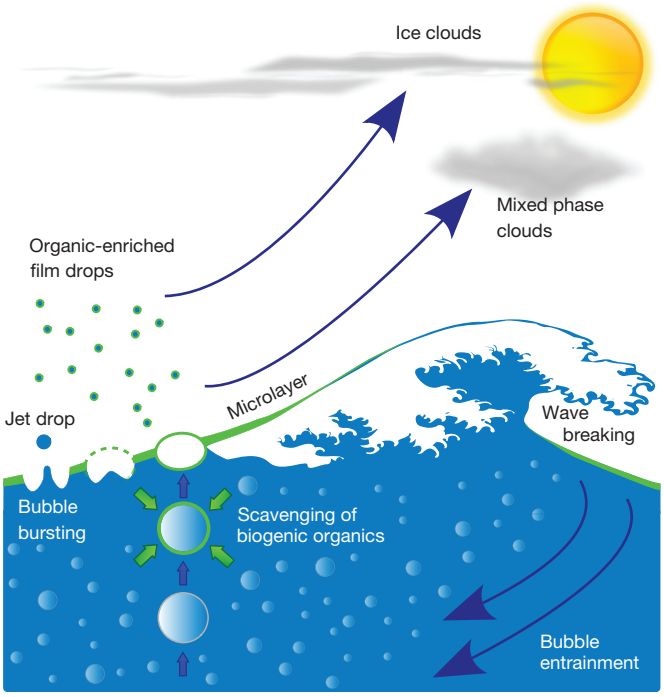

Figure 1 | Sea-spray aerosol particles enriched in organic material are generated when bubbles burst at the air–sea interface. Surface active organic material of biological origin is scavenged at the interfaces of bubbles as they rise through the water column. This process enriches the air–sea interface with surface active organic material forming the SML (green layers). The organic material is ejected on bubble bursting with resulting submicrometre film drops being enriched with organic material compared with larger jet drops. We show that the biogenic organic material in the SML is probably an important source of atmospheric INPs that could influence cloud properties.

[1]School of Earth and Environment, University of Leeds, Woodhouse Lane, Leeds LS2 9JT, UK. [2]Department of Chemistry, University of Toronto, 80 St George Street, Toronto, Ontario M5S 3H6, Canada. [3]Institute for Terrestrial and Planetary Atmospheres, School of Marine and Atmospheric Sciences, Stony Brook University, Stony Brook, New York 11794-5000, USA. [4]School of Biological Sciences, University of Essex, Colchester CO4 3SQ, UK. [5]Atmospheric Science and Global Change Division, Pacific Northwest National Laboratory, 902 Battelle Boulevard, Richland, Washington 99354, USA. [6]Department of Chemistry and Biochemistry, University of Denver, Denver, Colorado 80208, USA. [7]School of Marine and Atmospheric Sciences, Stony Brook University, Stony Brook, New York 11794-5000, USA. [8]Department of Chemistry, University of British Columbia, 2036 Main Mall, Vancouver, British Columbia V6T 1Z1, Canada. [9]School of Earth, Atmospheric and Environmental Sciences, University of Manchester, Manchester M13 9PL, UK. [10]Institute of Ocean Sciences, Fisheries and Oceans Canada, Sidney, British Columbia V8L 4B2, Canada. [11]Air Quality Science Unit, Environment Canada, Vancouver, British Columbia V6C 3S5, Canada. [12]Leibniz Institute for Baltic Sea Research Warnemünde, Department of Biological Oceanography, Seestraße 15, 18119 Rostock, Germany. †Present address: Carl-von-Ossietzky University Oldenburg, Institute of Chemistry and Biology of the Marine Environment, AG Meeresoberflächen, Emstrasse 20, 26382 Wilhelmshaven, Germany. *These authors contributed equally to this work.

containing similar organic material to that of the microlayer[12–19] (Fig. 1). Measurements of atmospheric INP concentrations in the remote oceans indicate that there may be a marine source of INPs linked to marine biology[3–5], and modelling work indicates that this may be important in mixed-phase clouds[9,10]. There is also evidence to suggest that ice nucleation in cirrus clouds over ocean regions is influenced by sea-spray aerosol, with about 25% of the heterogeneously nucleated ice particle residuals identified as sea salt[20]. Despite these indications that there is a marine source of atmospheric INPs, the SML has not previously been analysed for the presence of material capable of nucleating ice. To determine whether there is a source of atmospheric INPs in the microlayer, we examined the ice-nucleating properties of microlayer samples collected in the Arctic (July–August 2013), Atlantic (May–June 2014), North Pacific (June 2013), and in coastal locations off British Columbia, Canada (August 2013) (Extended Data Fig. 1).

First we present experiments relevant to mixed-phase clouds, in which 1 µl droplets of microlayer samples from the Arctic and Atlantic Oceans were placed on a cold stage immediately after sampling, and cooled until frozen. The fraction of droplets that froze as a function of temperature, corrected for freezing depression caused by salts, is shown in Fig. 2a. The microlayer droplets consistently froze at higher temperatures than droplets of subsurface water (SSW) collected at depths of between 2 to 5 m at the same locations (Extended Data Table 1). Filtration and re-testing of the microlayer samples showed that most material that nucleated ice was between approximately 0.2 and 0.02 µm in size (Extended Data Fig. 2a). Material of this size has the potential to be lofted into the atmosphere through bubble-bursting processes, forming atmospheric INPs that are internally mixed with sea salt and other organics. To estimate atmospheric INP concentrations associated with marine organics, we determined the number of these INPs present per mass of organic carbon (Fig. 2b; see Methods); this result is used in the modelling section of this paper.

Experiments were also conducted under conditions relevant to cirrus clouds using microlayer and SSW samples from the North Pacific and the British Columbia coast. The activity of the collected samples was tested at −40 °C and compared with results from experiments with commercial sea salt and NaCl particles. Figure 2c shows example activation curves for aerosolized, dried and size-selected (200 nm diameter) particles. The SSW activation curves are very similar to those of sea salt and NaCl, with all showing sharp increases above 143% relative humidity with respect to ice (RH_{ice}). This is consistent with homogeneous ice nucleation of solution droplets and suggests that crystalline salt particles did not contribute markedly to ice nucleation events observed at low RH_{ice}. In contrast, aerosol particles derived from microlayer samples all showed ice formation above the background level at lower RH_{ice}. The ice nucleation onset (RH_{ice} at which 1% of the aerosol particles were activated; Fig. 2d) varied between 115% and 133% RH_{ice}, which is comparable with efficient deposition mode INPs, such as Arizona test dust (ATD) and feldspar dust (orthoclase) particles of the same size[1,21]. Filtration of the SML samples through filters with nominal pore sizes of 0.2 µm increased the ice nucleation onset by about 12–16 ± 4% RH_{ice}, indicating that some ice active material larger than 0.2 µm was present (Extended Data Fig. 2b). However, the onsets for the 0.2-µm-filtered samples remained well below the homogeneous threshold, indicating that there is a population of smaller INPs in the British Columbia and Pacific microlayer samples, consistent with the Arctic and Atlantic data. The cumulative number of ice nucleation sites per surface area as a function of RH_{ice}, $n_s(RH_{ice})$, was greater for the microlayer samples than that found for ATD, kaolinite and feldspar mineral dusts[21,22] (Extended Data Fig. 3; see refs 1, 2 for more information on n_s).

We emphasize that owing to the different nucleation processes involved, ice nucleation under mixed-phase cloud and cirrus conditions cannot be quantitatively compared. However, our results do clearly show that the microlayers at all the sampling locations were enriched in INPs compared with the SSW at the same locations. Here

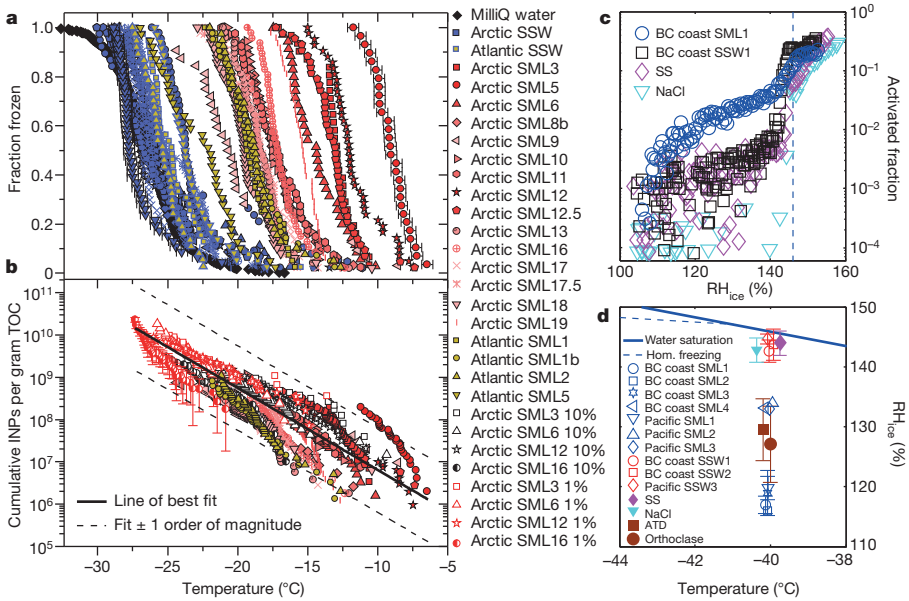

Figure 2 | Ice nucleation by material in the SML. **a**, Immersion mode fraction frozen curves for 1 µl Arctic and Atlantic SML and SSW droplets determined using the microlitre nucleation by immersed particle instrument (µl-NIPI), with example temperature uncertainties included. **b**, The cumulative number of INPs per gram of total organic carbon (TOC). Selected samples were diluted with ultrapure (MilliQ) water to 10% and 1% of initial concentration. Uncertainties are included where error bars are larger than data points (see Methods for details). Equation for fit to data is INPs per gram TOC = $\exp[11.2186 - (0.4459 \times T)]$; note that temperature, T, is in °C. **c**, Ice nucleation by British Columbia (BC) coast and North Pacific samples under cirrus conditions. Example University of Toronto continuous flow diffusion chamber (UT-CFDC) activation curves under cirrus conditions (with background counts subtracted) for sea salt (SS), NaCl, British Columbia coast SML and SSW samples at −40 °C. **d**, Ice nucleation onset RH_{ice} for Pacific and British Columbia coast SML, SSW, sea salt and NaCl aerosol particles. For comparison, onsets for ATD and K-feldspar (orthoclase)[21] are shown. Ice-onset error bars represent one standard deviation based on three to four replicates. The solid line represents the water saturation line, and the dashed line is the theoretical homogeneous freezing threshold[31].

we present experiments designed to reveal likely candidates for the source of the ice-nucleating activity.

Certain proteins have been identified as being highly ice active; however, heat denatures proteins, causing a reduction in activity, which is not the case for known inorganic INPs[2]. To test whether similar thermally labile material could be responsible for the observed ice nucleation, microlayer samples were heated at temperatures up to 100 °C and retested for activity. Heating of Arctic and Atlantic samples resulted in a reduction of the ice nucleation activity with freezing shifting to lower temperatures (Extended Data Fig. 2c). Similarly, the onset RH_{ice} of a British Columbia coast sample increased by $6 \pm 4\%$ RH_{ice}, whereas that of a Pacific sample was within uncertainty of the unheated sample (Extended Data Fig. 2b). This might be consistent with the presence of inorganic or other non-thermally labile INPs. The marked reduction in activity in samples from three out of four locations is consistent with the presence of thermally labile biological INPs.

The filtration tests on the sampled microlayers (mentioned earlier) show that there is a considerable population of INPs that pass through 0.2 µm filters (Extended Data Fig. 2a, b). The ice active materials are therefore probably smaller biological particles, for example, ultramicrobacteria, viruses or extracellular material from phytoplankton or bacteria (exudate). Additionally, no correlation was found between freezing temperature and bacterial cell counts in the Arctic microlayer (Extended Data Fig. 4), which suggests that whole bacterial cells were not responsible for the observed ice nucleation. Given that terrestrial biological systems such as pollens[23,24] and fungi[25,26] have been found to produce nanoscale or 'macromolecular' INPs unconnected with whole cells, we considered the possibility that marine INPs are associated with exudates from phytoplankton or other marine microorganisms. This hypothesis is not only supported by the filtration tests, but by a tentative correlation between the North Pacific microlayer sample ice activation onsets with both the dissolved organic carbon concentration (DOC; >0.2 µm) and polysaccharide-rich transparent exopolymer particles (TEPs), which are associated with phytoplankton exudates (Extended Data Fig. 5).

Qualitative compositional analysis of two Arctic samples using scanning transmission X-ray microscopy coupled with near edge absorption fine structure spectroscopy (STXM/NEXAFS; Fig. 3a–c) indicates the presence of both diatom cell wall and exudate compounds (see Methods). Spectra of exudates from the ubiquitous marine diatom *T. pseudonana*[27] share absorption features with the microlayer samples. These data are in keeping with studies showing that diatom exudates are present in microlayer samples[18] and consistent with the fact that diatoms are the dominant phytoplanktonic group in polar regions[28].

Diatom cells and fragments have been shown to nucleate ice heterogeneously[6] but, as demonstrated, whole cells are not solely responsible for the ice nucleation activity we observe in the microlayer samples. Here we investigate whether exudates separated from *T. pseudonana* diatom cells can nucleate ice heterogeneously. The ice nucleation efficiency of exudate from an axenic unialgal culture of *T. pseudonana* filtered through a 0.1 µm filter was measured as a function of temperature and water activity (a_w) in nanolitre volume droplets. Exudate freezing temperatures were found to be similar to those of washed diatom cells in the absence of exudate material and approximately 9–13 °C warmer than observed homogeneous freezing temperatures of 0.2-µm-filtered and autoclaved Atlantic sea water collected 100 km offshore of Long Island, New York (the same water used to culture diatoms) with and without added nutrients (Fig. 3d; freezing curves are shown in Extended Data Fig. 6). While the freezing temperatures shown in Fig. 3d are not directly comparable to the microlayer droplet experiments in Fig. 2a, as they used much smaller droplets, they do show that material associated with exudates can nucleate ice.

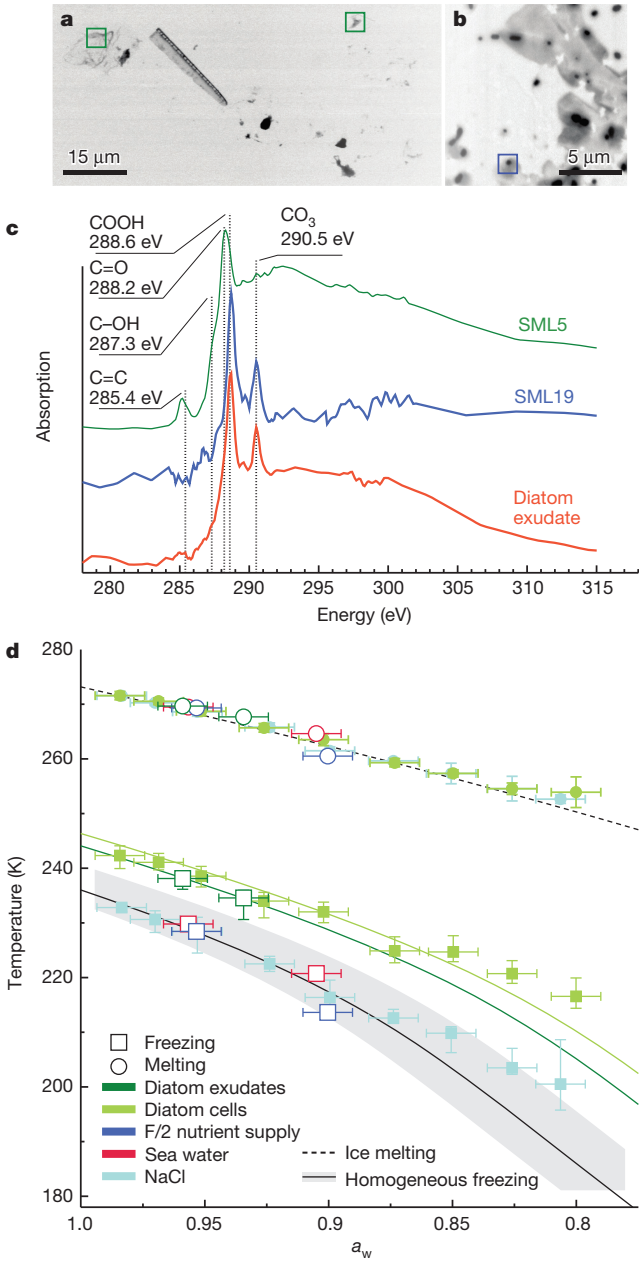

Figure 3 | Spectroscopic analysis of Arctic SML samples and freezing experiments with diatom exudate. **a**, **b**, X-ray images of Arctic SML5 (**a**) and SML19 (**b**). Example locations at which spectra were acquired are indicated by green and blue boxes. **c**, X-ray absorption spectra of organic material in SML5, SML19 and exudates from the diatom *T. pseudonana*. **d**, Freezing and melting temperatures, collected using the water-activity-controlled immersion freezing experiment (WACIFE), as a function of water activity (a_w) for nanolitre volume droplets containing *T. pseudonana* exudates, and filtered and autoclaved natural sea water with and without f/2 nutrients. Heterogeneous ice nucleation temperatures in the presence of diatom cells and homogeneous ice nucleation of aqueous NaCl droplets are shown for comparison[6,32]. Vertical error bars represent 10th and 90th percentiles of about 300 individual freezing events. Horizontal error bars indicate the uncertainty in a_w of ±0.01.

Given the ice nucleation activity of exudates from *T. pseudonana*, the presence of similar material in Arctic microlayer samples and the results of the filtering and heating experiments, we suggest that biogenic INPs present in phytoplankton exudates are a good candidate for the source of activity observed in the sampled microlayers. A substantial mass fraction of submicrometre sea-spray aerosol is

organic material[12,16], which is often associated with phytoplankton exudates[16,29]. Our results indicate therefore that some fraction of sea-spray aerosol particles will be capable of nucleating ice.

To explore the possible contribution of marine biogenic INP sources to the global atmospheric INP distribution, we combined our experimental data with the modelled distribution of emitted primary organic material in sea-spray aerosol[10] (Fig. 4a; see Methods for details). To calculate atmospheric INP concentrations, we assume that the organic component of sea-spray aerosol simulated by the model has a temperature-dependent INP concentration (per mass of organic carbon) equal to that measured in the Arctic and Atlantic samples (Fig. 2b). In other words, the number of INPs is directly related to the mass of organic carbon computed by the model. At our current level of understanding, this can be considered as an estimate for the number of INPs present in the organic component of sea-spray aerosol. The predicted surface-level marine organic INP concentrations ($[INP]_{-15}$; the concentration of INPs if an air parcel were cooled to −15 °C at water saturation) are also shown in Fig. 4a. The largest concentrations of marine INPs occur over the Southern Oceans, the North Atlantic and the North Pacific in regions where biological activity in surface ocean waters and wind speeds are greatest. Comparison of the simulated annual mean marine INP concentrations at sea level agree within ±1 order of magnitude with the Bigg[3] atmospheric INP measurements in the Southern Ocean and around the coast of Australia (Fig. 4b), while mineral dust from deserts (the major terrestrial INP source) only accounts for a small fraction of the observed INPs in this region. We also find good agreement with measurements made previously[4] in the southern Pacific. We note that some of the INP measurements made in the equatorial Pacific[4] tend to be underpredicted by our model, implying either another source of INPs or a stronger marine INP source than predicted here, possibly related to short-term variability in ocean biota.

We also use the model to assess the transport of marine INPs to altitudes relevant for mixed-phase clouds. Figure 4c shows the concentration of INPs active at −20 °C from marine sources at 850 hPa in comparison with the contribution from desert dusts based on K-feldspar distributions[30]. This suggests that marine biogenic sources of INPs are competitive with, or more important than, desert sources in large parts of the Southern Ocean, the North Atlantic and the North Pacific. To assess whether marine organic INPs exist in regions of the atmosphere that are sufficiently cold for them to activate to ice, we plot 3-monthly averaged seasonal distributions of INPs active at the ambient temperature ($[INP]_{ambient}$) along a transect through the Atlantic (at 30° W; Fig. 4d). This plot suggests that marine organic sea spray may contribute markedly to cloud glaciation at high and mid latitudes during the wintertime in the respective hemispheres. It also shows the strong seasonal differences caused by temperature and source strength to the relative $[INP]_{ambient}$ contribution from marine and dust sources.

We show that surface active organic material from the microlayer that is similar to that found in sea-spray aerosol nucleates ice, and we tentatively identify the ice active material as being connected to diatom exudates. Our findings also suggest that marine organic material may be an important global source of atmospheric INPs, particularly in areas remote from terrestrial sources such as the Southern Ocean. This work highlights the need for more field measurements of remote atmospheric INP concentration and investigation of its relationship with ocean surface water characteristics, including the local phytoplankton community, organic carbon concentrations and

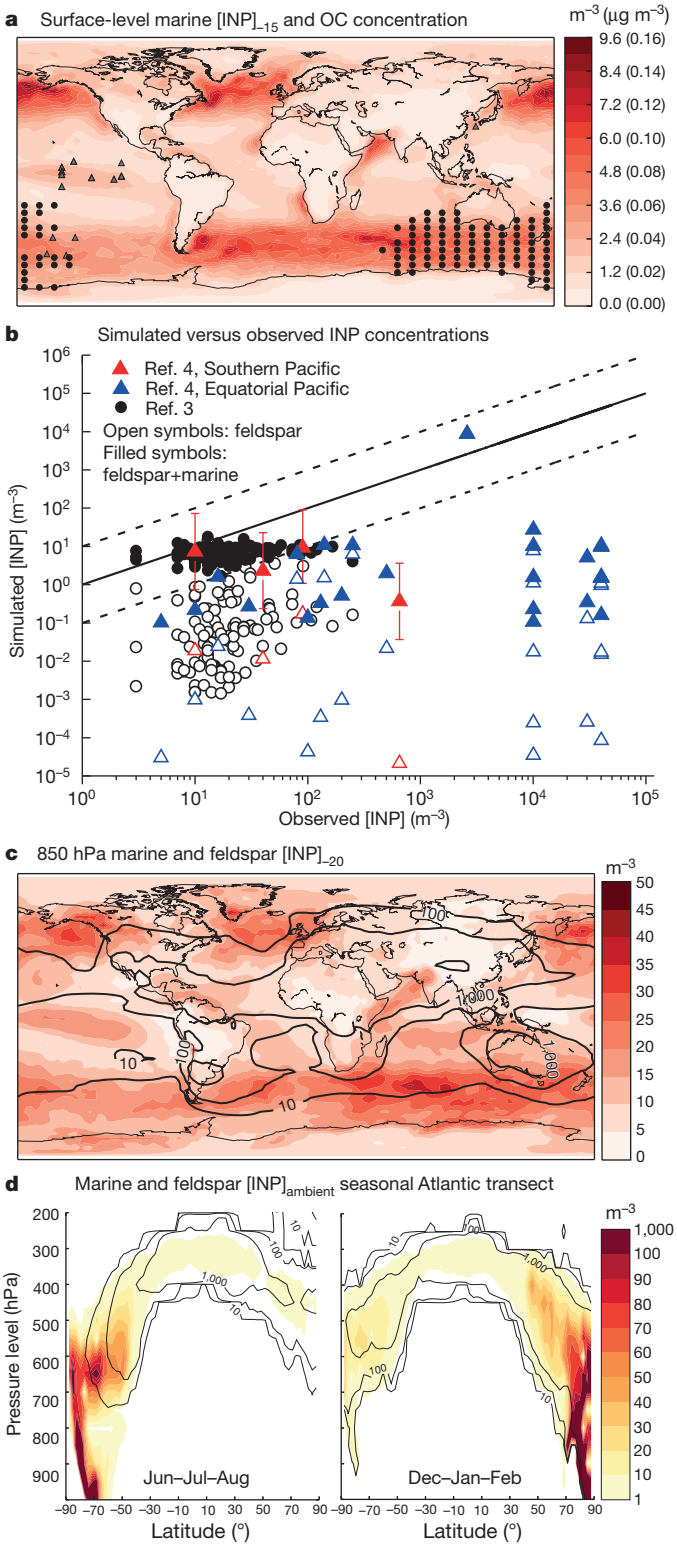

Figure 4 | Global distribution of atmospheric marine biogenic INPs. **a**, Modelled distribution of INP concentration active at −15 °C (m^{-3}) and surface-level marine aerosol organic mass concentration (μg m^{-3}); the locations of Bigg[3] (circles) and Rosinski[4] (triangles) data are shown. **b**, Comparison of model-simulated INP concentration versus the Bigg[3] and Rosinski[4] measured concentrations for the same location at the activation temperature of the measurements; open symbols are for K-feldspar only and filled symbols are for mineral dust plus marine organic. Example error bars shown on red points are based on spread in INPs per gram TOC (see Fig. 2b). **c**, Modelled distribution of marine biogenic INP concentrations active at −20 °C at 850 hPa (corresponding to the altitude of high-latitude mixed-phase clouds). Black contours indicate the INPs from desert dust based on K-feldspar emissions[30]. **d**, Seasonal altitude profiles (expressed as pressure) showing $[INP]_{ambient}$ (INP concentration active at local temperature conditions) from marine sources (colour scale) and K-feldspar (black contours), for a transect from the South to North poles through the Atlantic (30 °W).

chemical characteristics, as well as the organic loading and nature of sea-spray aerosol.

Online Content Methods, along with any additional Extended Data display items and Source Data, are available in the online version of the paper; references unique to these sections appear only in the online paper.

Received 9 October 2014; accepted 17 July 2015.

1. Hoose, C. & Möhler, O. Heterogeneous ice nucleation on atmospheric aerosols: a review of results from laboratory experiments. *Atmos. Chem. Phys.* **12,** 9817–9854 (2012).
2. Murray, B. J., O'Sullivan, D., Atkinson, J. D. & Webb, M. E. Ice nucleation by particles immersed in supercooled cloud droplets. *Chem. Soc. Rev.* **41,** 6519–6554 (2012).
3. Bigg, E. K. Ice nucleus concentrations in remote areas. *J. Atmos. Sci.* **30,** 1153–1157 (1973).
4. Rosinski, J., Haagenson, P. L., Nagamoto, C. T. & Parungo, F. Nature of ice-forming nuclei in marine air masses. *J. Aerosol Sci.* **18,** 291–309 (1987).
5. Bigg, E. K. Ice forming nuclei in the high Arctic. *Tellus* **B48,** 223–233 (1996).
6. Knopf, D. A., Alpert, P. A., Wang, B. & Aller, J. Y. Stimulation of ice nucleation by marine diatoms. *Nature Geosci.* **4,** 88–90 (2011).
7. Fall, R. & Schnell, R. C. Association of an ice-nucleating psuedomonad with cultures of the marine dinoflagellate, *Heterocapsa niei*. *J. Mar. Res.* **43,** 257–265 (1985).
8. Prather, K. A. *et al.* Bringing the ocean into the laboratory to probe the chemical complexity of sea spray aerosol. *Proc. Natl Acad. Sci. USA* **110,** 7550–7555 (2013).
9. Yun, Y. & Penner, J. E. An evaluation of the potential radiative forcing and climatic impact of marine organic aerosols as heterogeneous ice nuclei. *Geophys. Res. Lett.* **40,** 4121–4126 (2013).
10. Burrows, S. M., Hoose, C., Pöschl, U. & Lawrence, M. G. Ice nuclei in marine air: biogenic particles or dust? *Atmos. Chem. Phys.* **13,** 245–267 (2013).
11. Wang, X. *et al.* Microbial control of sea spray aerosol composition: a tale of two blooms. *ACS Cent. Sci.* **1,** 124–131 (2015).
12. Gantt, B. & Meskhidze, N. The physical and chemical characteristics of marine primary organic aerosol: a review. *Atmos. Chem. Phys.* **13,** 3979–3996 (2013).
13. Aller, J. Y., Kuznetsova, M. R., Jahns, C. J. & Kemp, P. F. The sea surface microlayer as a source of viral and bacterial enrichment in marine aerosols. *J. Aerosol Sci.* **36,** 801–812 (2005).
14. Orellana, M. V. *et al.* Marine microgels as a source of cloud condensation nuclei in the high Arctic. *Proc. Natl Acad. Sci. USA* **108,** 13612–13617 (2011).
15. Schmitt-Kopplin, P. *et al.* Dissolved organic matter in sea spray: a transfer study from marine surface water to aerosols. *Biogeosciences* **9,** 1571–1582 (2012).
16. Russell, L. M., Hawkins, L. N., Frossard, A. A., Quinn, P. K. & Bates, T. S. Carbohydrate-like composition of submicron atmospheric particles and their production from ocean bubble bursting. *Proc. Natl Acad. Sci. USA* **107,** 6652–6657 (2010).
17. Leck, C. & Bigg, E. K. Biogenic particles in the surface microlayer and overlaying atmosphere in the central Arctic Ocean during summer. *Tellus* **B57,** 305–316 (2005).
18. Cunliffe, M. *et al.* Sea surface microlayers: a unified physicochemical and biological perspective of the air–ocean interface. *Prog. Oceanogr.* **109,** 104–116 (2013).
19. Quinn, P. K. *et al.* Contribution of sea surface carbon pool to organic matter enrichment in sea spray aerosol. *Nature Geosci.* **7,** 228–232 (2014).
20. Cziczo, D. J. *et al.* Clarifying the dominant sources and mechanisms of cirrus cloud formation. *Science* **340,** 1320–1324 (2013).
21. Yakobi-Hancock, J. D., Ladino, L. A. & Abbatt, J. P. D. Feldspar minerals as efficient deposition ice nuclei. *Atmos. Chem. Phys.* **13,** 11175–11185 (2013).
22. Kanji, Z. A., Welti, A., Chou, C., Stetzer, O. & Lohmann, U. Laboratory studies of immersion and deposition mode ice nucleation of ozone aged mineral dust particles. *Atmos. Chem. Phys.* **13,** 9097–9118 (2013).
23. Pummer, B. G., Bauer, H., Bernardi, J., Bleicher, S. & Grothe, H. Suspendable macromolecules are responsible for ice nucleation activity of birch and conifer pollen. *Atmos. Chem. Phys.* **12,** 2541–2550 (2012).
24. Augustin, S. *et al.* Immersion freezing of birch pollen washing water. *Atmos. Chem. Phys.* **13,** 10989–11003 (2013).
25. O'Sullivan, D. *et al.* The relevance of nanoscale biological fragments for ice nucleation in clouds. *Sci. Rep.* **5,** 8082 (2015).
26. Fröhlich-Nowoisky, J. *et al.* Ice nucleation activity in the widespread soil fungus *Mortierella alpina*. *Biogeosciences* **12,** 1057–1071 (2015).
27. Armbrust, E. V. The life of diatoms in the world's oceans. *Nature* **459,** 185–192 (2009).
28. Alvain, S., Moulin, C., Dandonneau, Y. & Loisel, H. Seasonal distribution and succession of dominant phytoplankton groups in the global ocean: a satellite view. *Glob. Biogeochem. Cycles* **22,** GB3001 (2008).
29. Fuentes, E., Coe, H., Green, D. & McFiggans, G. On the impacts of phytoplankton-derived organic matter on the properties of the primary marine aerosol—part 2: composition, hygroscopicity and cloud condensation activity. *Atmos. Chem. Phys.* **11,** 2585–2602 (2011).
30. Atkinson, J. D. *et al.* The importance of feldspar for ice nucleation by mineral dust in mixed-phase clouds. *Nature* **498,** 355–358 (2013).
31. Koop, T., Luo, B., Tsias, A. & Peter, T. Water activity as the determinant for homogeneous ice nucleation in aqueous solutions. *Nature* **406,** 611–614 (2000).
32. Alpert, P. A., Aller, J. Y. & Knopf, D. A. Ice nucleation from aqueous NaCl droplets with and without marine diatoms. *Atmos. Chem. Phys.* **11,** 5539–5555 (2011).

Acknowledgements T.W.W., B.J.M. and T.F.W. acknowledge the assistance provided by the crew and other scientists onboard the R/V *Knorr* and the RRS *James Clark Ross*, the British Antarctic Survey, K. Baustian, J. McQuaid, A. Windross, J. Knulst, J. F. Wilson, A. M. Booth, R. Chance, L. J. Carpenter, S. Peppe, D. O'Sullivan, N. Umo, I. Cotton, H. Pearce, H. Price and M. J. Callaghan. The STXM/NEXAFS analysis was performed at the Advanced Light Source (ALS), Lawrence Berkeley National Laboratory supported by the Director, Office of Science, Office of Basic Energy Sciences, of the US Department of Energy under contract no. DE-AC02-05CH11231 (user award to D.A.K./J.Y.A. ALS-05955). STXM analyses were facilitated by A. L. D. Kilcoyne and M. K. Gilles. L.A.L. acknowledges assistance from R. Leaitch, E. Mungall, R. Christensen and J. Li, and the Pacific region Department of Fisheries and Oceans staff. The Marine Boundary Layer sampling site in Ucluelet is jointly supported and maintained by Environment Canada, the British Columbia Ministry of the Environment and Metro Vancouver. We acknowledge funding from the Natural Environment Research Council (NE/K004417/1, NE/I020059/1, NE/I013466/1, NE/I028696/1, NE/I019057/1, NE/H009485/1), the European Research Council (FP7, 240449 ICE, BACCHUS 603445), the UK Aerosol Society, National Science Foundation (AGS-1232203), German Research Foundation (WU585/6-1), the Climate Change and Atmospheric Research Program of the Natural Sciences and Engineering Research Council of Canada (for NETCARE), Fisheries and Oceans Canada, Environment Canada, NOAA's Climate Program Office (for WACS II), and the DOE Office of Science (BER) Earth System Modeling Program.

Author Contributions T.W.W. organized the ICE-ACCACIA campaign, designed experiments, collected and analysed samples during and after the campaign, managed collaborations and co-wrote this manuscript. L.A.L. designed experiments and analysed samples during the NETCARE campaign and co-wrote this manuscript. P.A.A. collected and analysed STXM/NEXAFS spectra and diatom exudate freezing data and contributed to manuscript writing. M.N.B. collected flow cytometry data for SML samples during ACCACIA. I.M.B. sought funding for ACCACIA and helped design the microlayer sampling procedure. S.M.B., J.V.T., J.B. and K.S.C. performed and analysed the model simulations. C.J. performed heating tests on ICE-ACCACIA samples. W.P.K. assisted with collection of material during the WACS II cruise, provided exudate material for experiments, and participated in STXM/NEXAFS data collection. G.M., J.J.N. and S.R. conducted total organic carbon measurements on Arctic samples. L.A.M., O.W. and E.P. collected the Ucluelet, Line P and open ocean samples, and conducted the NETCARE biogeochemical analysis. C.L.S. helped organize the measurements at the Ucluelet site and facilitated the use of the sampling site. T.F.W. collected and analysed samples during and after the ICE-ACCACIA campaign and assisted with design of experiments. J.D.Y.-H., J.A.H., R.H.M., M.S. and J.P.S.W. collected the Ucluelet samples and helped with the NETCARE experiments. A.K.B. and J.P.D.A. oversaw and organized the NETCARE field campaign and provided financial support for it. D.A.K. and J.Y.A. initiated and designed the STXM/NEXAFS and diatom exudate freezing experiments, contributed to the writing of this manuscript and provided financial support for WACS II cruise participation, exudate freezing experiments, and STXM/NEXAFS analyses. B.J.M. established the collaborations necessary for this paper, helped to write the paper and oversaw the ICE-ACCACIA campaign and sought funding for it.

Author Information Reprints and permissions information is available at www.nature.com/reprints. The authors declare no competing financial interests. Readers are welcome to comment on the online version of the paper. Correspondence and requests for materials should be addressed to T.W.W. (theo.w.wilson@gmail.com) or L.A.L. (luis.ladinomoreno@utoronto.ca).

METHODS

SML and SSW sampling. SML sampling took place in the Arctic during the Aerosol-Cloud Coupling and Climate Interactions in the Arctic (ACCACIA) cruise, in the Atlantic as part of the Western Atlantic Climate Study II (WACS II) cruise, as well as in the Northeast Pacific and off the southern coast of British Columbia, Canada, as part of the Network on Climate and Aerosols: Addressing Key Uncertainties in Remote Canadian Environments (NETCARE) project (Extended Data Fig. 1). See Extended Data Table 1 for precise sampling locations.

During the ACCACIA campaign in the Arctic, microlayer sampling was conducted from the RRS *James Clark Ross* in both open waters and within leads in the marginal ice zone (Extended Data Table 1 and Extended Data Fig. 1a). Microlayer samples were collected into borosilicate glass bottles from a hydrophilic Teflon film on a rotating drum fitted to the 'Interface II' remote-controlled sampling catamaran[33]. SSW was sampled with Niskin bottles on a CTD (conductivity, temperature, depth) rig at the same locations, generally at a depth of ~2 m. To avoid potential contamination from the ship, the microlayer sampler was navigated to a distance of 75–200 m upwind of the stationary ship before sampling commenced. Owing to rougher conditions during the WACS II campaign in the Atlantic, the Interface II was tethered to the CTD arm of the R/V *Knorr* during microlayer sampling. SSW was collected either using the direct uncontaminated ship input at 5-m water depth or using a sampling container lowered over the side of the ship (for details see Extended Data Table 1). During both campaigns, before and after microlayer sampling, sea water from the ship's uncontaminated supply was flushed through Interface II's sampling system to clear any previously collected microlayer. Samples of the 'flushing' water were collected and analysed and compared to the SSW using droplet freezing assays to check that INPs from previous sampling had been removed (Extended Data Fig. 8). Microlayer samples for water activity and organic carbon analysis were frozen immediately after collection at −80 °C.

During the NETCARE campaign, SML samples and corresponding SSW samples from water depths of 0.5–1.0 m were collected in the Northeast Pacific Ocean at three different locations (Extended Data Table 1 and Extended Data Fig. 1c). The samples were collected using a glass plate[34] with the exception of British Columbia (BC) coast SML3, which was collected using an autoclaved stainless steel screen[18]. All samples were stored in high-density polyethylene bottles. North Pacific samples (Pacific SML1, 2 and 3) were kept frozen at −20 °C after collection, and before the experiment they were thawed and stored at 4 °C in the dark. All other samples were stored at 4 °C in the dark for no more than 10 days before analysis.

Effect of different sampling techniques on INP abundance in Pacific samples. BC coast samples SML3 and SML4 were sampled at the same location 1 h apart but using metal mesh and glass plate techniques, respectively. There is a significant difference in the onset humidity of the two samples, with the onset of ice formation for BC coast SML3 occurring 13% RH_{ice} lower than for BC coast SML4. With the time lag between collection of the two samples and because the methods sample different thicknesses of the SML (the metal plate collects layers 2–4 times thicker than those layers collected with glass plates[18]), it is not clear if the difference in their onset RH_{ice} was due to the different sampling methods.

Ice nucleation experiments during ACCACIA, WACS II and NETCARE. Arctic and Atlantic SML and SSW samples were analysed for the presence of INPs using the previously described[30,35] microlitre nucleation by immersed particle instrument (μl-NIPI). Briefly, droplets with a volume of 1.0 ± 0.1 μl were pipetted onto a hydrophobic microscope coverslip (Extended Data Fig. 9a) and cooled at a rate of 1 K min^{-1} using a Grant-Asymptote EF600 cold stage (Extended Data Fig. 9b) until all droplets were frozen. The temperature at which individual droplets froze was recorded, with an uncertainty of ±0.4 °C. Experiments were also performed using diluted microlayer samples (Arctic SML3, 6, 16 plus Arctic SML5 filtered at 0.2 μm and Arctic SML12 filtered at 10 μm), where 1 ml of microlayer was added to 9 ml (10% dilution) or 99 ml (1% dilution) of 18.2 MΩ cm distilled water (Milli-Q). The water activity (a_w) of Arctic microlayer and SSW samples was measured at 25 °C using an Aqualab Series 3 dew point activity meter.

Samples from the North Pacific and BC coast were analysed using the University of Toronto continuous flow diffusion chamber (UT-CFDC). Owing to the high total submicrometre particle concentration of both the microlayer and SSW samples (10^6 cm^{-3} after drying, measured with a TSI 3782 condensation particle counter) they were diluted by a factor of approximately 20 with 18.2 MΩ cm water before atomization using a TSI 3076 atomizer. Water was removed by passing the sample flow through three diffusion dryers, and the particle concentration was further lowered by dilution (Extended Data Fig. 9c). Two-hundred-nanometre mobility diameter particles were selected using a differential mobility analyser (TSI 3081), with size-selected particle concentrations of approximately 100 cm^{-3}. The size-selected particles were exposed to ice supersaturated conditions at −40 °C in the UT-CFDC to determine their ice nucleation onset humidities[36]. Particle counts from both channels (>0.5 μm and >5 μm) of the optical particle counter (Climet CI-20) were used to distinguish between interstitial aerosol particles and ice particles. The standard solutions consisted of 8–10 mg of NaCl (Sigma Aldrich, S2830) and commercial sea salt (Sigma Aldrich, S9883) dissolved in 50 ml of 18.2 MΩ cm water. Control experiments with filtered air were conducted in the field.

Ice nucleation experiments with diatom exudates. For diatom exudate freezing experiments, axenic unialgal cultures of *T. pseudonana* were grown in flasks at 16–18 °C with a 14 h light:10 h dark cycle in 0.1-μm-filtered and autoclaved sea water with f/2 nutrient addition[37]. Sea water was collected at a depth of about 0.5 m about 100 km off the coast of Long Island, New York[38]. After 1 week of growth, when concentrations reached ~10^6 cells ml^{-1}, cultures were filtered through a 0.1 μm pore size filter to remove the cells, yielding a suspension of diatom exudates.

Droplets of filtered diatom exudate were analysed using the water-activity-controlled immersion freezing experiment (WACIFE) instrument. Individual droplets were deposited in a grid pattern onto a hydrophobic glass plate. Additional droplets were generated from filtered and autoclaved natural sea water with and without f/2 nutrient addition[37] before diatom growth. Droplet a_w was established by allowing the temperature-controlled droplets to come to equilibrium in a humidity-controlled aerosol conditioning cell[6,39]. Droplets were then sealed from ambient air, setting the droplets' a_w equal to the applied RH. Ice nucleation was observed at a cooling rate of 10 K min^{-1} using a cryo-cooling stage coupled to an optical microscope (see schematic of process in Extended Data Fig. 9d). Droplet sizes ranged from 60 to 129 μm circle equivalent diameters (82 μm average). Individual droplet volumes were calculated from the spherical equivalent diameter derived from the digitally measured particle diameters corrected for the non-sphericity of the deposited particles and for different applied a_w. The total number of droplets at each investigated a_w for sea water, sea water plus f/2 droplets, and sea water plus f/2 plus diatom exudates were 115, 143 and 131, respectively. Homogeneous ice nucleation was observed for droplets generated from the sea water with and without f/2. The median freezing temperatures shown in Fig. 3d include 10th and 90th percentiles. Corresponding mean melting temperatures are shown with an uncertainty of 1 standard deviation. The uncertainty in a_w is ±0.01. The ice melting curve (dashed line) and the volume-corrected homogeneous freezing curve with an uncertainty in a_w of ±0.01 shown as the solid black line and grey shaded area, respectively, are parameterized as described previously[40].

Freezing depression correction for immersion mode experiments. Data from the Arctic, Atlantic and diatom exudate immersion mode experiments were adjusted to account for the freezing depression caused by dissolved salts in sea water. First, a freezing curve as a function of a_w was constructed through the median freezing points following the a_w criterion where median immersion freezing temperatures can be described by a horizontal shift in the ice melting curve[40]. Then the difference between expected median freezing temperatures for pure water (that is, at $a_w = 1.0$) and at the experimentally applied a_w were used as temperature offsets.

Calculation of INPs per gram of organic carbon and associated uncertainty. In Fig. 2b we show the cumulative number of INPs per gram of TOC as a function of temperature for the Arctic and Atlantic microlayer samples. This calculation uses the time-independent singular description of ice nucleation[41] that assumes the time dependence of freezing is of secondary importance to the distribution of ice nucleating particle types. In this case 'INPs per gram of TOC' is the same as 'n_m' described in detail elsewhere[2]. It should also be noted that this is the same model that was used to calculate n_s (ref. 1) for the BC coast and North Pacific samples, but this describes the number of ice active sites per surface area rather than mass.

For all data points shown in Fig. 2b, error bars are based on the propagated uncertainties associated with volume measurements and organic carbon concentration measurements (Extended Data Fig. 7). The error bars for experiments in which microlayer samples were diluted with Milli-Q water also include uncertainty relating to the subtraction of background heterogeneous nucleation events.

Freezing in μl-NIPI experiments using Milli-Q water droplets free from any added nucleants occurs at higher temperatures than predicted for homogeneous ice nucleation[42]. Using the results of 22 separate freezing experiments (727 droplets in total) the cumulative number of INPs per volume of Milli-Q was calculated. A line of best fit from this data as a function of temperature was used to estimate the number of background INPs present in our diluted microlayer samples. This value was subtracted from the diluted microlayer cumulative INP spectra and uncertainties relating to the variation in background INP concentrations were calculated based on the 68% confidence interval associated with the line of best fit.

STXM/NEXAFS analysis of Arctic microlayer samples. STXM/NEXAFS analysis was used to explore qualitatively the carbon functionality of organic material found in two Arctic SML samples (Arctic SML5 and 19). Analyses were performed at the Advanced Light Source on beamline 5.3.2.2, Lawrence Berkeley National

Laboratory[43]. Overviews of the application of this technique to atmospheric particles and technical details on STXM methodology have been published elsewhere[44–50].The sample for STXM/NEXAFS analysis was collected by bringing the flat face of clean silicon nitride windows into contact with the pre-collected SML water surface and then lifting them off. Material adhering to the windows was allowed to air dry before examination. The transmission of soft single-energy X-ray photons across the raster-scanned sample was measured to obtain an image[43] exploiting the carbon K-edge spectra to identify carbon functionality and the overall contribution of inorganic components. Using X-ray energies 278–320 eV, X-ray absorption of the ground state electron (1*s* orbital) of the carbon atom was probed to identify carbon–carbon double bonding (C=C), carbonyl (C=O), hydroxyl (C–OH) and carboxyl (COOH) functional groups. Figure 3a shows an X-ray image of particulate material found in the Arctic SML5 sample taken at 320 eV, which includes organic and inorganic material and a frustule fragment. The spectrum for SML5 is characterized by (1) a dominant carbonyl peak (288.2 eV), (2) a secondary carbon double-bonding peak (285.4 eV), and (3) a gradual rise in absorption in the energy range where the hydroxyl functional group absorbs (287.3 eV). Similar spectra for diatom cell wall material have previously been observed[51]. The spectrum observed from SML19 is similar to that of the spectrum obtained from diatom exudates and is characterized by (1) a dominant carboxyl peak (288.6 eV) and (2) a gradual rise in absorption in the energy range where the hydroxyl functional group absorbs (287.3 eV). Similar spectral features have been observed previously[52] for field-collected marine particles, which the authors attributed to the presence of polysaccharides, and also[53] for particles aerosolized from a laboratory breaking wave. These features were also observed in carbon absorption spectra[54] for 22 amino acids, all of which are present in *T. pseudonana*[55], supporting the notion that diatom exudates were present in this microlayer sample. The presence of spectral features similar to diatom cell wall fragments and diatom exudate material suggests the presence of diatoms in both SML5 and SML19. It is important to note that marine SMLs[13,18,56–58], SSWs[59] and biofilms[60] are comprised of a complex mixture of inorganic particles, particulate organic matter in the form of microorganisms, biogenic debris, polysaccharide enriched microgels, lipids, proteins and amino acids. Therefore, the X-ray spectra shown here will not be identical for different SML samples. Instead, key spectral features including peak locations and dominance, represent typical biogenically derived materials in the marine environment.

Microlayer filtering and heating tests. A selection of fresh Arctic SML samples were passed through filters with a range of pore sizes (0.02 μm Whatman Anodisc, 0.1 μm Whatman Anodisc, 0.2 μm Sartorius Minisart, 0.45 μm Sartorius Minisart, 2.0 μm Millipore TTTP) and then tested for changes in immersion mode ice nucleating activity (Extended Data Fig. 2a). Selected NETCARE samples were filtered through 0.2 μm polyethersulfone membranes (IC Acrodisc) and then retested under cirrus conditions for ice nucleation activity (Extended Data Fig. 2b).

Selected Arctic and Atlantic samples were tested for immersion freezing activity after having been heated in a temperature-controlled bath for 10 min. This was repeated at 8 temperatures between 20 °C and 100 °C (Extended Data Fig. 2c). NETCARE samples, BC coast SML3 and Pacific SML1 were heated for 10 min at 100 °C and retested under cirrus conditions for ice nucleation activity (Extended Data Fig. 2b).

Flow cytometry for ACCACIA SML samples. Samples (2 ml) were transferred into a cryovial, and 50 μl of 50% glutaraldehyde was added to achieve a 0.5% solution. The preserved sample was stored in the refrigerator for 30 min before snap-freezing in liquid nitrogen for storage at −80 °C. Prior to analysis, samples were defrosted and the nucleic acid stain SYBR Green 1 dissolved in 300 mM potassium nitrate solution was added to achieve a 1% concentration of the stain (see refs 61 and 62 for more details). The samples were kept in the dark at room temperature for 1 h. Bacterial abundance shown in Extended Data Fig. 4 was quantified using a flow cytometer (Becton Dickinson FACScan) following methods outlined in the literature[61,62].

TOC, DOC and TEP characterization. Transparent exopolymer particle (TEP; Extended Data Fig. 5b) concentrations were determined using spectrophotometric methods[63]. Samples (5–50 ml) of NETCARE SML and SSW were filtered immediately after sampling onto 0.2 μm polycarbonate membranes under low vacuum pressure (<100 mm Hg) and the membranes were stained with 0.5 ml Alcian blue solution (0.02 g Alcian blue in 100 ml of acetic acid solution, pH 2.5), and rinsed twice with 1 ml of deionized water. Membranes were subsequently extracted in 6 ml of 80% sulfuric acid (H_2SO_4) for 2 h to dissolve the dye, and the absorbance of extracts was measured in a 1 cm cuvette at 787 nm with standardization using xanthan gum equivalents (X_{eq}) and conversion to μg C l^{-1} using a factor of 0.63 based on the compilation of multiple studies using phytoplankton cultures[64].

For analysis of DOC[65] in the NETCARE samples from the North Pacific (Extended Data Fig. 5a), subsamples of 20 ml were filtered through 0.2 μm polycarbonate membranes and the filtrates preserved for later analysis with 4 μl H_3PO_4 per ml sample. Concentrations of DOC were quantified using a Shimadzu TOC-V analyser.

Organic carbon analysis was also performed on the Arctic microlayer samples (Extended Data Fig. 7). After filtering through 0.2 μm pore size Whatman Anodisc filters, DOC was measured using a Shimadzu TOC-V using previously described methods[66,67]. Owing to high carbon concentration the Arctic microlayer samples for total organic carbon (TOC) analysis were diluted with one part sample to two parts deionized water. Total carbon analyser (TOC 5050A, Shimadzu) was used to measure total organic and inorganic carbon in each sample twice (with coefficient of variance between measurements <2%); the average of these measurements was taken.

Atlantic samples were also analysed for DOC; 40 ml of sample was filtered through a 25 mm GFF filter and stored in a glass septum bottle. The resulting supernatant was acidified to a pH of 1 with roughly 3 drops of pure HCl to react with any inorganic carbon, and inhibit potential microbial degradation before analysis in the DOC analyser (Shimadzu TOC-L, ±1% precision). Prior to DOC collection each septum bottle and filtration apparatus was acid washed, and GFF filters were pre-combusted for 5 h at 450 °C. Particulate organic carbon (POC) was measured in Atlantic samples by filtering SML through pre-combusted 25 mm GFF filters (0.7 μm pore size) before analysis (filters were frozen at −20 °C until processing).

Global modelling study. To assess the potential contribution of marine biogenic INP sources to the global atmospheric INP distribution, we combined our experimental data from immersion mode experiments using the Arctic and Atlantic SML samples (the fit shown in Fig. 2b) with a modelled distribution of emitted primary organic material in sea-spray aerosol[10]. This was compared to desert dust INP concentrations based on emissions of K-feldspar[30].

Atmospheric marine POC distributions are taken from ref. 10. Briefly, organic material (OM) in sea spray is related to emitted NaCl by an empirical, observationally based enrichment factor $(OM_{aerosol}/NaCl_{aerosol})/(OM_{sea}/NaCl_{sea}) = 500$. Furthermore, the OM fraction in emitted sea spray $(OM_{aerosol}/(OM_{aerosol} + NaCl_{aerosol}))$ was not allowed to exceed 76%; which was the maximum observed submicrometre organic sea spray fraction according to ref. 68. Marine organic carbon is emitted in proportion to climatological POC as retrieved by the MODIS-Aqua satellite, transported as soluble $r = 100$ nm particles in the atmosphere, and removed by size-dependent wet and dry deposition processes. The OM distribution (using OM = OC × 1.9) was shown previously[10] to be consistent with another global model study of atmospheric marine OM[68] and is within a factor of two of annual mean atmospheric measurements at Amsterdam Island (37°48′ S, 77°34′ E)[69] and Mace Head (53°20′ N, 9°54′ W)[68].

The distribution of dust INPs was based on a previous study[30], which used the global aerosol processes model (GLOMAP). In this study we used GLOMAP-mode[70], a two-moment aerosol size-resolving scheme, which calculates particle mass and number in seven variable-size log-normal modes. The model is forced by ECMWF 6-hourly global meteorological analyses and was run at a resolution of 2.8 × 2.8, with 31 pressure levels extending to ~10 hPa. Dust emissions are taken from the AEROCOM daily resolved dust inventory for 2000 (ref. 71). Emissions are separated into a feldspar and bulk component using a mineralogical inventory[72]. Dust is emitted into the insoluble (or primary) size distribution and is aged to the soluble distribution via condensation of SO_2 and secondary organics after which it is subject to wet scavenging processes. Evaluation of modelled dust mass concentrations against surface observations (from the University of Miami network) show a model bias of ~30% with the majority of observations within a factor of 2 of the modelled mass[70].

Mineral dust INP concentrations (originating from K-feldspar) were calculated offline via the time independent model as discussed previously[30]. K-Feldspar (assumed to be 35% of Feldspar volume) surface area and particle number was calculated assuming external mixing within the soluble modes.

Figure 4d shows seasonal modelled concentrations of marine (colour scale) and K-feldspar (contours) INPs that are active at the ambient model temperature. We refer to this concentration as $[INP]_{ambient}$ and it is a useful indicator of locations in which INP concentrations are sufficiently high and the temperatures sufficiently low to potentially influence clouds. Both marine and K-feldspar $[INP]_{ambient}$ were calculated using averaged daily temperatures and averaged monthly marine organic and K-feldspar emissions during the indicated periods (left panel, December–January–February; right panel, June–July–August). In both cases the parameterizations used are valid over a limited temperature range (see Fig. 2b for marine INP, and ref. 30 for K-feldspar). We did not extrapolate for INP concentrations at temperatures above the upper limits of the parameterization, instead we assumed the aerosol had no ice-nucleating activity at higher temperatures. Owing to the INP numbers being cumulative as temperature decreases, the concentration of INPs at the lowest valid temperature of the parameterizations represent the lower limits for INP concentrations at temperatures colder than the valid range.

Below −38 °C we do not show $[INP]_{ambient}$ since in this regime homogeneous nucleation will dominate.

33. Knulst, J. C., Rosenberger, D., Thompson, B. & Paatero, J. Intensive sea surface microlayer investigations of open leads in the pack ice during Arctic Ocean 2001 expedition. *Langmuir* **19,** 10194–10199 (2003).
34. Wurl, O., Miller, L., Röttgers, R. & Vagle, S. The distribution and fate of surface-active substances in the sea-surface microlayer and water column. *Mar. Chem.* **115,** 1–9 (2009).
35. Whale, T. F. *et al.* A technique for quantifying heterogeneous ice nucleation in microlitre supercooled water droplets. *Atmos. Meas. Tech.* **8,** 2437–2447 (2015).
36. Kanji, Z. A. & Abbatt, J. P. D. The University of Toronto Continuous Flow Diffusion Chamber (UT-CFDC): a simple design for ice nucleation studies. *Aerosol Sci. Technol.* **43,** 730–738 (2009).
37. Guillard, R. R. L. & Ryther, J. H. Studies of marine planktonic diatoms. I. *Cyclotella nana* Hustedt, and *Detonula confervacea* (cleve) Gran. *Can. J. Microbiol.* **8,** 229–239 (1962).
38. Fisher, N. S. & Wente, M. The release of trace elements by dying marine phytoplankton. *Deep-Sea Res. I* **40,** 671–694 (1993).
39. Alpert, P. A., Aller, J. Y. & Knopf, D. A. Initiation of the ice phase by marine biogenic surfaces in supersaturated gas and supercooled aqueous phases. *Phys. Chem. Chem. Phys.* **13,** 19882–19894 (2011).
40. Koop, T. & Zobrist, B. Parameterizations for ice nucleation in biological and atmospheric systems. *Phys. Chem. Chem. Phys.* **11,** 10839–10850 (2009).
41. Vali, G. Quantitative evaluation of experimental results an the heterogeneous freezing nucleation of supercooled liquids. *J. Atmos. Sci.* **28,** 402–409 (1971).
42. Murray, B. J. *et al.* Kinetics of the homogeneous freezing of water. *Phys. Chem. Chem. Phys.* **12,** 10380–10387 (2010).
43. Kilcoyne, A. L. D. *et al.* Interferometer-controlled scanning transmission X-ray microscopes at the Advanced Light Source. *J. Synchrotron Radiat.* **10,** 125–136 (2003).
44. Ghorai, S., Laskin, A. & Tivanski, A. V. Spectroscopic evidence of keto-enol tautomerism in deliquesced malonic acid particles. *J. Phys. Chem. A* **115,** 4373–4380 (2011).
45. Ghorai, S. & Tivanski, A. V. Hygroscopic behavior of individual submicrometer particles studied by X-ray spectromicroscopy. *Anal. Chem.* **82,** 9289–9298 (2010).
46. Moffet, R. C., Henn, T., Laskin, A. & Gilles, M. K. Automated chemical analysis of internally mixed aerosol particles using X-ray spectromicroscopy at the carbon K-edge. *Anal. Chem.* **82,** 7906–7914 (2010).
47. Moffet, R. C. & Tivanski, A. V & Gilles, M. K. in *Fundamentals and Applications of Aerosol Spectroscopy* (eds Signorell, R. & Reid, J. P.) 419–462 (Taylor & Francis Group, 2010).
48. Hopkins, R. J., Tivanski, A. V., Marten, B. D. & Gilles, M. K. Chemical bonding and structure of black carbon reference materials and individual carbonaceous atmospheric aerosols. *J. Aerosol Sci.* **38,** 573–591 (2007).
49. Knopf, D. A. *et al.* Microspectroscopic imaging and characterization of individually identified ice nucleating particles from a case field study. *J. Geophys. Res. Atmos.* **119,** 10365–10381 (2014).
50. Takahama, S., Gilardoni, S., Russell, L. M. & Kilcoyne, A. L. D. Classification of multiple types of organic carbon composition in atmospheric particles by scanning transmission X-ray microscopy analysis. *Atmos. Environ.* **41,** 9435–9451 (2007).
51. Abramson, L., Wirick, S., Lee, C., Jacobsen, C. & Brandes, J. A. The use of soft X-ray spectromicroscopy to investigate the distribution and composition of organic matter in a diatom frustule and a biomimetic analog. *Deep-Sea Res. II* **56,** 1369–1380 (2009).
52. Hawkins, L. N. & Russell, L. M. Polysaccharides, proteins, and phytoplankton fragments: four chemically distinct types of marine primary organic aerosol classified by single particle spectromicroscopy. *Adv. Meteorol.* **2010,** 612132 (2010).
53. Ault, A. P. *et al.* Size-dependent changes in sea spray aerosol composition and properties with different seawater conditions. *Environ. Sci. Technol.* **47,** 5603–5612 (2013).
54. Zubavichus, Y., Shaporenko, A., Grunze, M. & Zharnikov, M. Innershell absorption spectroscopy of amino acids at all relevant absorption edges. *J. Phys. Chem. A* **109,** 6998–7000 (2005).
55. Brown, M. R. The amino-acid and sugar composition of 16 species of microalgae used in mariculture. *J. Exp. Mar. Biol. Ecol.* **145,** 79–99 (1991).
56. Kuznetsova, M., Lee, C. & Aller, J. Characterization of the proteinaceous matter in marine aerosols. *Mar. Chem.* **96,** 359–377 (2005).
57. van Pinxteren, M., Müller, C., Iinuma, Y., Stolle, C. & Herrmann, H. Chemical characterization of dissolved organic compounds from coastal sea surface microlayers (Baltic Sea, Germany). *Environ. Sci. Technol.* **46,** 10455–10462 (2012).
58. Verdugo, P. Marine microgels. *Annu. Rev. Mar. Sci.* **4,** 375–400 (2012).
59. Brandes, J. A. *et al.* Examining marine particulate organic matter at sub-micron scales using scanning transmission X-ray microscopy and carbon X-ray absorption near edge structure spectroscopy. *Mar. Chem.* **92,** 107–121 (2004).
60. Lawrence, J. R. *et al.* Scanning transmission X-ray, laser scanning, and transmission electron microscopy mapping of the exopolymeric matrix of microbial biofilms. *Appl. Environ. Microbiol.* **69,** 5543–5554 (2003).
61. Marie, D., Partensky, F., Jacquet, S. & Vaulot, D. Enumeration and cell cycle analysis of natural populations of marine picoplankton by flow cytometry using the nucleic acid stain SYBR Green I. *Appl. Environ. Microbiol.* **63,** 186–193 (1997).
62. Zubkov, M. V., Burkill, P. H. & Topping, J. N. Flow cytometric enumeration of DNA-stained oceanic planktonic protists. *J. Plankton Res.* **29,** 79–86 (2007).
63. Engel, A. in *Practical Guidelines for the Analysis of Seawater* (ed. Wurl, O.) 125–142 (CRC Press, 2009).
64. Engel, A. Distribution of transparent exopolymer particles (TEP) in the northeast Atlantic Ocean and their potential significance for aggregation processes. *Deep-Sea Res. I* **51,** 83–92 (2004).
65. Wurl, O. & Sin, T. in *Practical Guidelines for the Analysis of Seawater* (ed. Wurl, O.) 33–48 (CRC Press, 2009).
66. Pan, X. *et al.* Dissolved organic carbon and apparent oxygen utilization in the Atlantic Ocean. *Deep-Sea Res. I* **85,** 80–87 (2014).
67. MacGilchrist, G. A. *et al.* Effect of enhanced pCO_2 levels on the production of dissolved organic carbon and transparent exopolymer particles in short-term bioassay experiments. *Biogeosciences* **11,** 3695–3706 (2014).
68. Vignati, E. *et al.* Global scale emission and distribution of sea-spray aerosol: sea-salt and organic enrichment. *Atmos. Environ.* **44,** 670–677 (2010).
69. Sciare, J. *et al.* Long-term observations of carbonaceous aerosols in the Austral Ocean atmosphere: Evidence of a biogenic marine organic source. *J. Geophys. Res. Atmos.* **114,** D15302 (2009).
70. Mann, G. W. *et al.* Description and evaluation of GLOMAP-mode: a modal global aerosol microphysics model for the UKCA composition-climate model. *Geosci. Model Dev.* **3,** 519–551 (2010).
71. Huneeus, N. *et al.* Global dust model intercomparison in AeroCom phase I. *Atmos. Chem. Phys.* **11,** 7781–7816 (2011).
72. Nickovic, S., Vukovic, A., Vujadinovic, M., Djurdjevic, V. & Pejanovic, G. Technical note: high-resolution mineralogical database of dust-productive soils for atmospheric dust modeling. *Atmos. Chem. Phys.* **12,** 845–855 (2012).

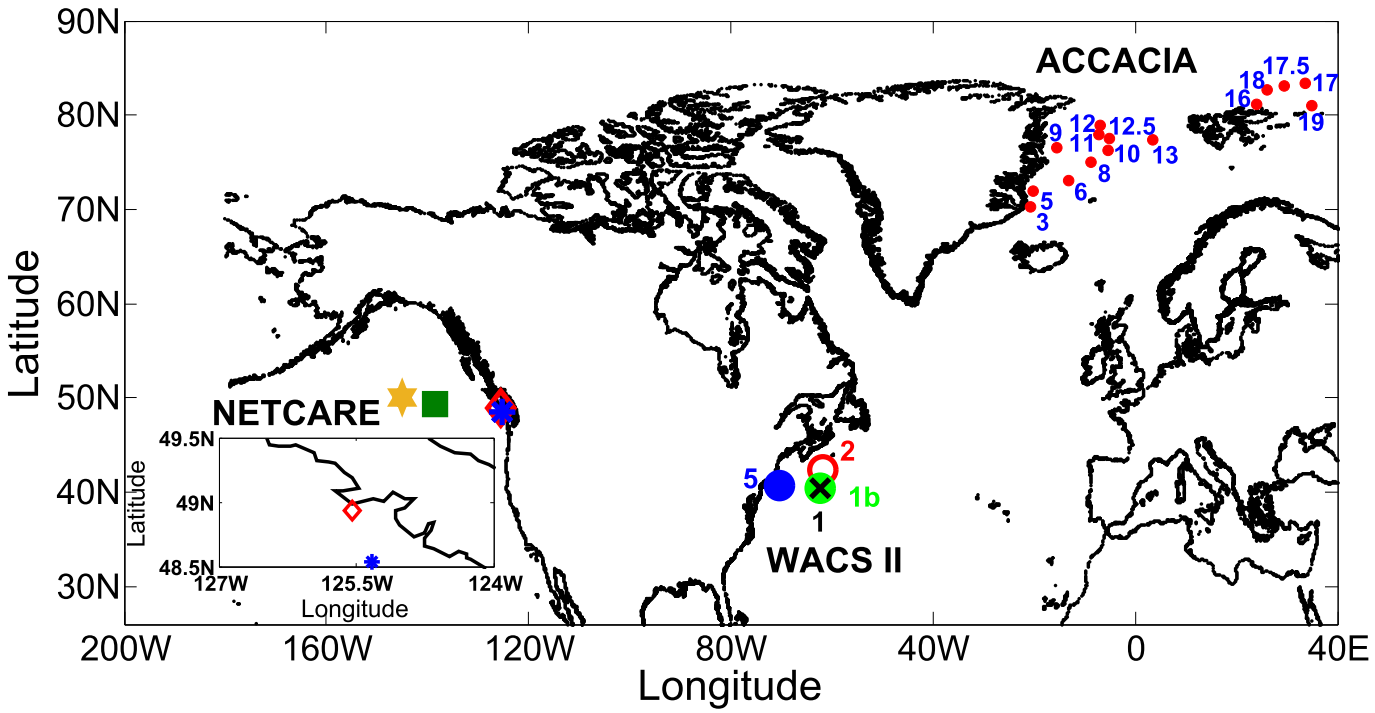

Extended Data Figure 1 | Sampling locations. SML and SSW samples were collected during the ACCACIA campaign (July–August 2013) at Arctic sampling stations at the locations marked with solid red circles. Also shown are sampling locations during the WACS II campaign (May–June 2014) in the North Atlantic Ocean. NETCARE samples were collected at locations in the Northeast Pacific (yellow star and green square, CCGS *John P. Tully*, 14–19 June 2013). The red diamond and blue asterisk correspond to the sampling locations for the NETCARE British Columbia (BC) coastal samples (12–15 August 2013). The inset is a zoom of the BC coast sampling locations.

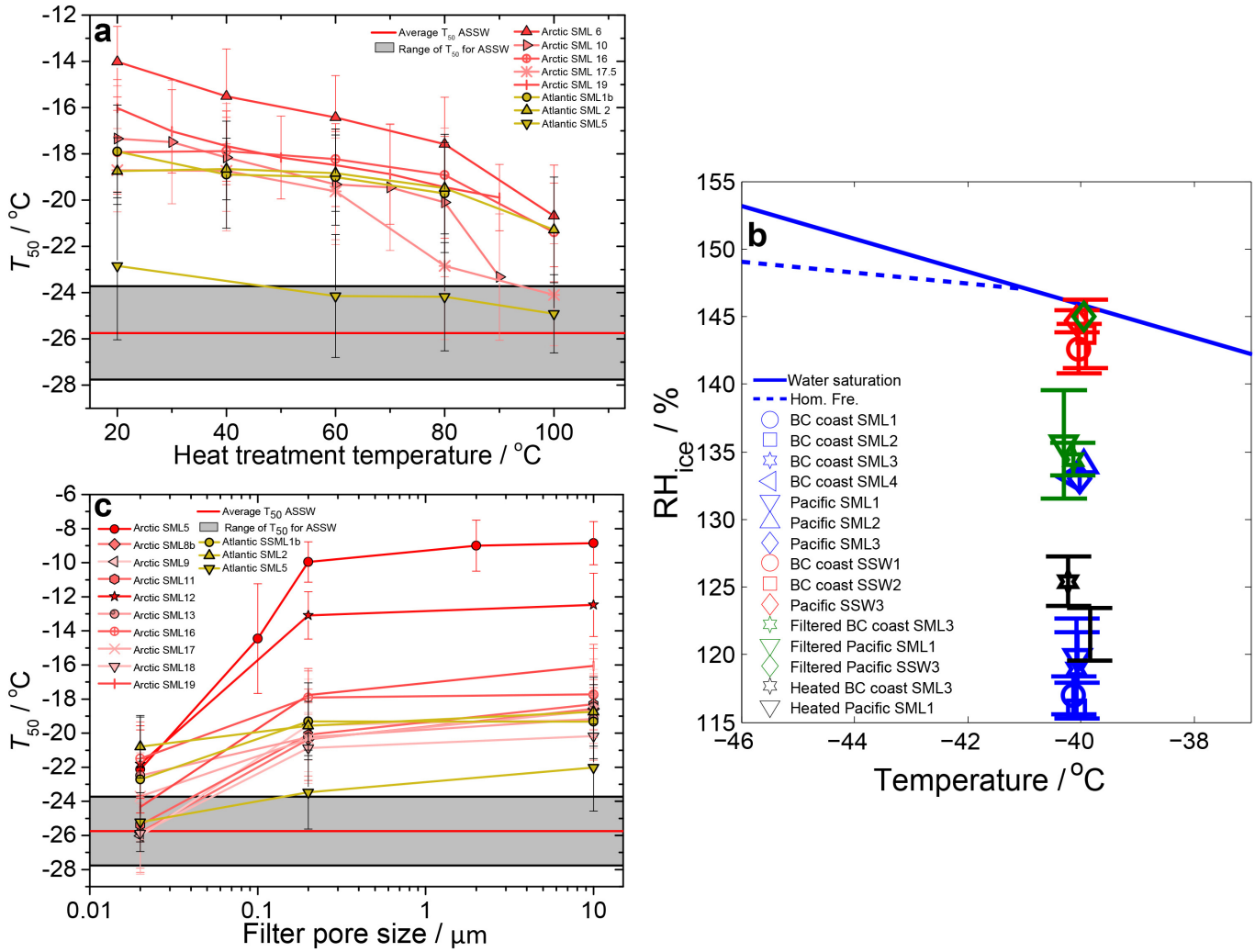

Extended Data Figure 2 | Effects of heating and filtering on the ice nucleation activity of microlayer samples. **a**, The effect of filtering through different pore-sized filters on the temperature at which 50% of droplets had frozen (T_{50}) of Arctic and Atlantic SML samples tested using the µl-NIPI. Error bars represent ± the standard deviation calculated from the freezing temperatures in each experiment, which consisted of between 30 and 53 individual events. Shaded grey area is the range of T_{50} found for fresh unfiltered SSW during the campaign. **b**, Comparison of the UT-CFDC onset RH_{ice} of unfiltered, filtered (0.2 µm) and heated (to 100 °C for 10 min) North Pacific and BC coast SML and SSW samples. The blue lines, and the red and dark blue symbols are as shown in Fig. 2d. The green symbols represent the filtered onsets, whereas the black symbols represent the heated results. Ice-nucleation-onset error bars represent one standard deviation based on three to four replicates. **c**, Results of heating tests using Arctic and Atlantic SML samples on T_{50} tested using the µl-NIPI. Error bars represent ± the standard deviation calculated from the freezing temperatures in each experiment, which consisted of between 28 and 46 individual events. Shaded grey area is the range of T_{50} found for fresh untreated Arctic SSW.

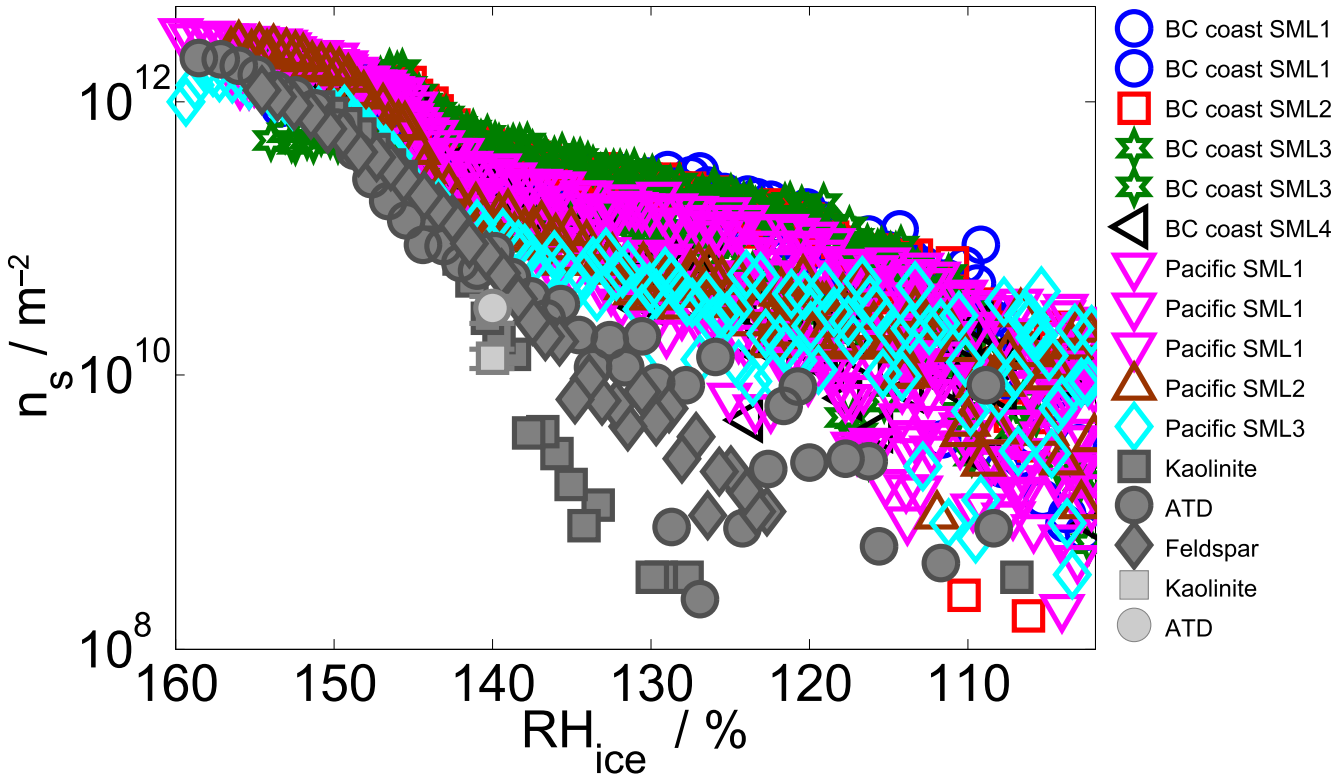

Extended Data Figure 3 | Ice surface site densities for the Pacific microlayer samples. Comparison of the ice surface densities (n_s) calculated from UT-CFDC data for the NETCARE SML samples with literature data. The n_s values were obtained at −40 °C assuming that the particles were spherical. The SML n_s values are indicated by the coloured symbols, whereas the mineral dust n_s values are indicated by the grey symbols. The dark grey and light grey symbols are from refs 21 and 22, respectively.

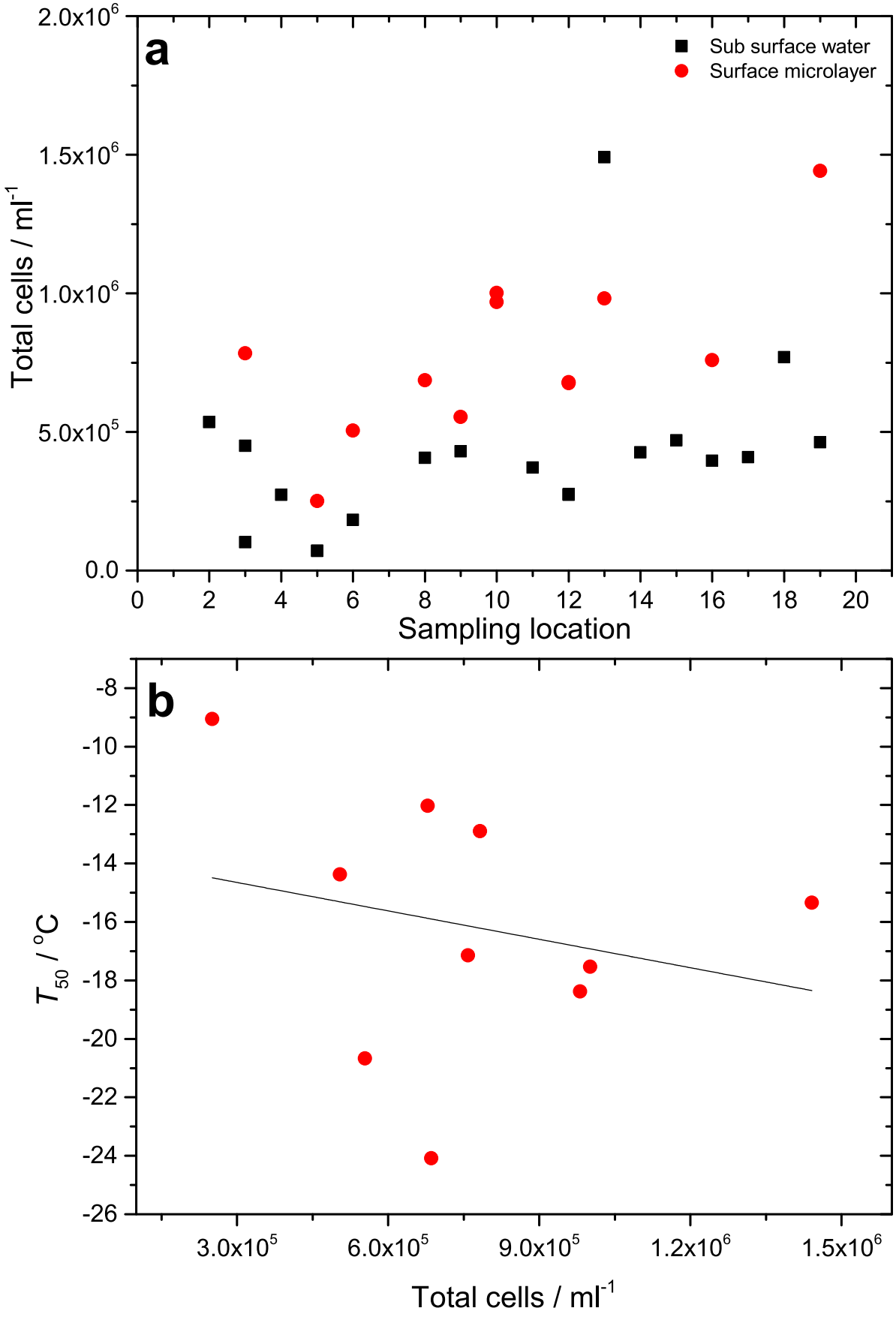

Extended Data Figure 4 | Bacterial cell counts for Arctic samples. **a**, Bacterial cell counts from flow cytometry performed on Arctic SSW (black squares), fresh Arctic SML (red circles). **b**, The SML sample cell counts plotted against T_{50} (temperature at which 50% of droplets frozen) and line of best fit, $R^2 = 0.29$.

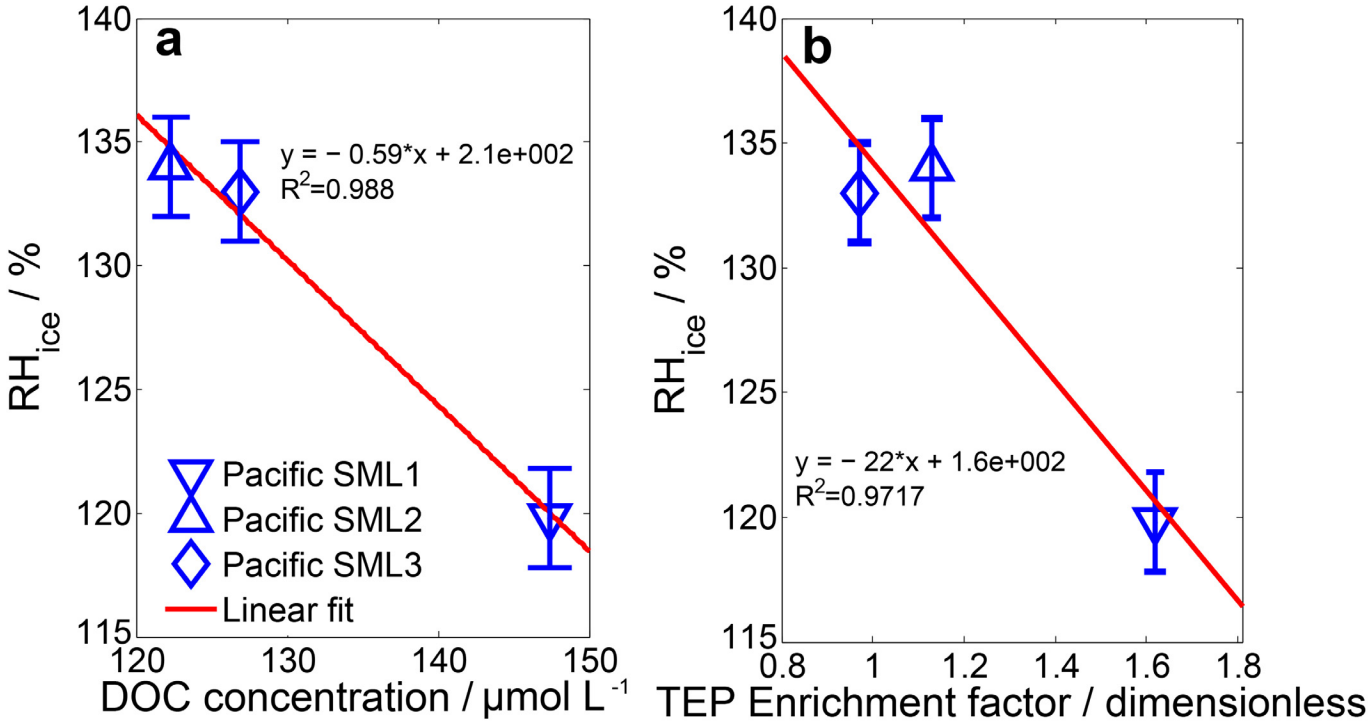

Extended Data Figure 5 | Correlation of TEP and DOC with the UT-CFDC RH_{ice} onsets. **a**, **b**, Ice nucleation RH_{ice} onsets for Northeast Pacific (see Extended Data Table 1) samples plotted against measured DOC concentration (**a**) and TEP enrichment factor (**b**). Error bars represent the experimental uncertainty in relative humidity with respect to ice in the UT-CFDC.

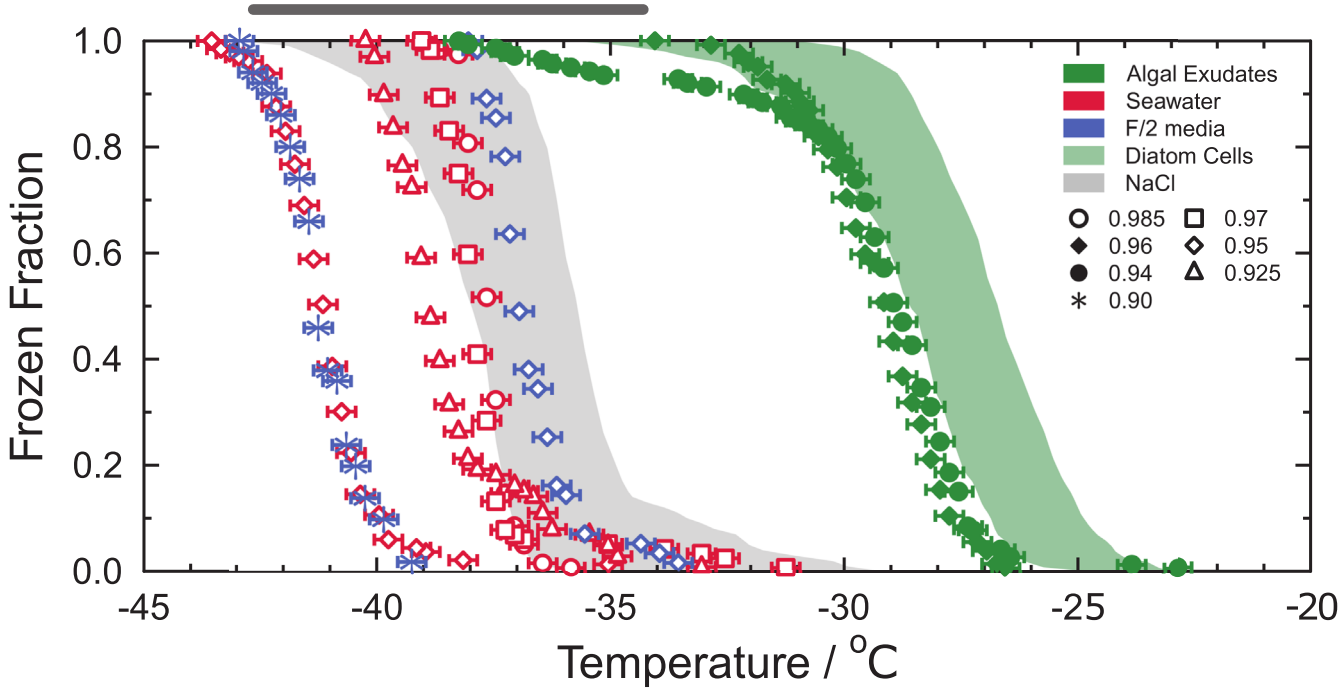

Extended Data Figure 6 | Ice-nucleating activity of diatoms cells and their exudates. WACIFE frozen fraction curves derived from 60–129-µm-sized droplets (~0.4 nl volume) as a function of temperature. Green symbols indicate diatom exudates in 0.1-µm-filtered sea water. Blue and red symbols represent 0.1-µm-filtered sea water devoid of exudates with and without the addition of growth media, respectively. All temperatures have been corrected for freezing point depression to pure water conditions from their initial aqueous solution water activity, a_w = 0.985 (open circles), 0.97 (open squares), 0.96 (filled diamonds), 0.95 (open diamonds), 0.94 (filled circles), 0.925 (open triangle), 0.90 (asterisks). Shaded areas illustrate ranges of observed heterogeneous ice nucleation of intact and fragmented diatom cells (green) and homogeneous ice nucleation of aqueous NaCl droplets (grey) for similar a_w values[6,32]. Error bars represent the instrumental uncertainty in temperature measurement. Predicted homogeneous freezing temperatures for similar sized water droplets are indicated by the grey bar[31,40].

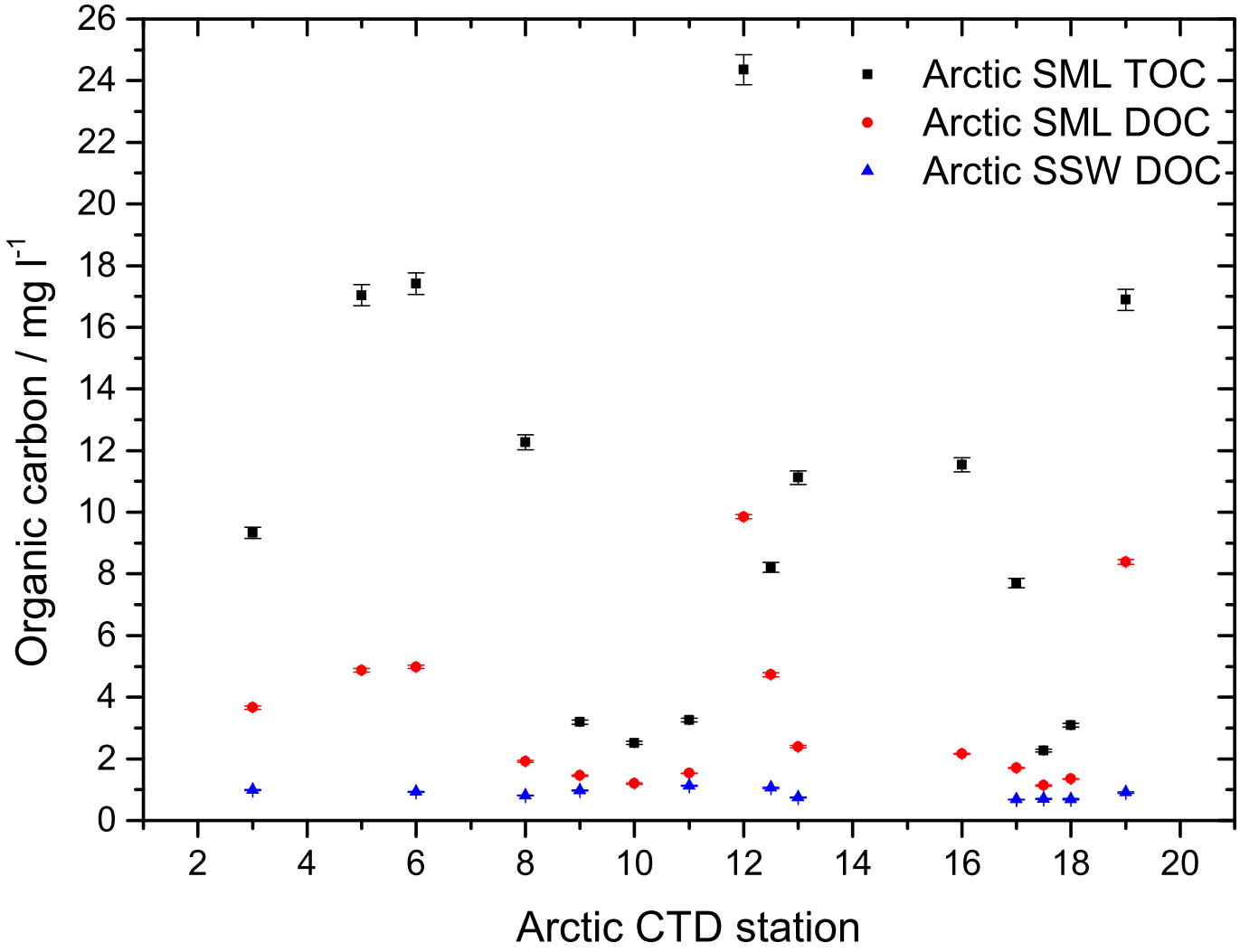

Extended Data Figure 7 | TOC and DOC measurements for Arctic samples. Arctic SML TOC and DOC measurements and Arctic SSW DOC measurements. TOC error bars represent the measured 2% coefficient of variance. DOC sample error was calculated as the coefficient of variation from the mean and standard deviation of three sample replicates. For comparison here we provide the Atlantic TOC measurements; Atlantic SML1 = 5.954 ± 0.185 mg l^{-1}, Atlantic SML2 = 4.643 ± 0.135 mg l^{-1}.

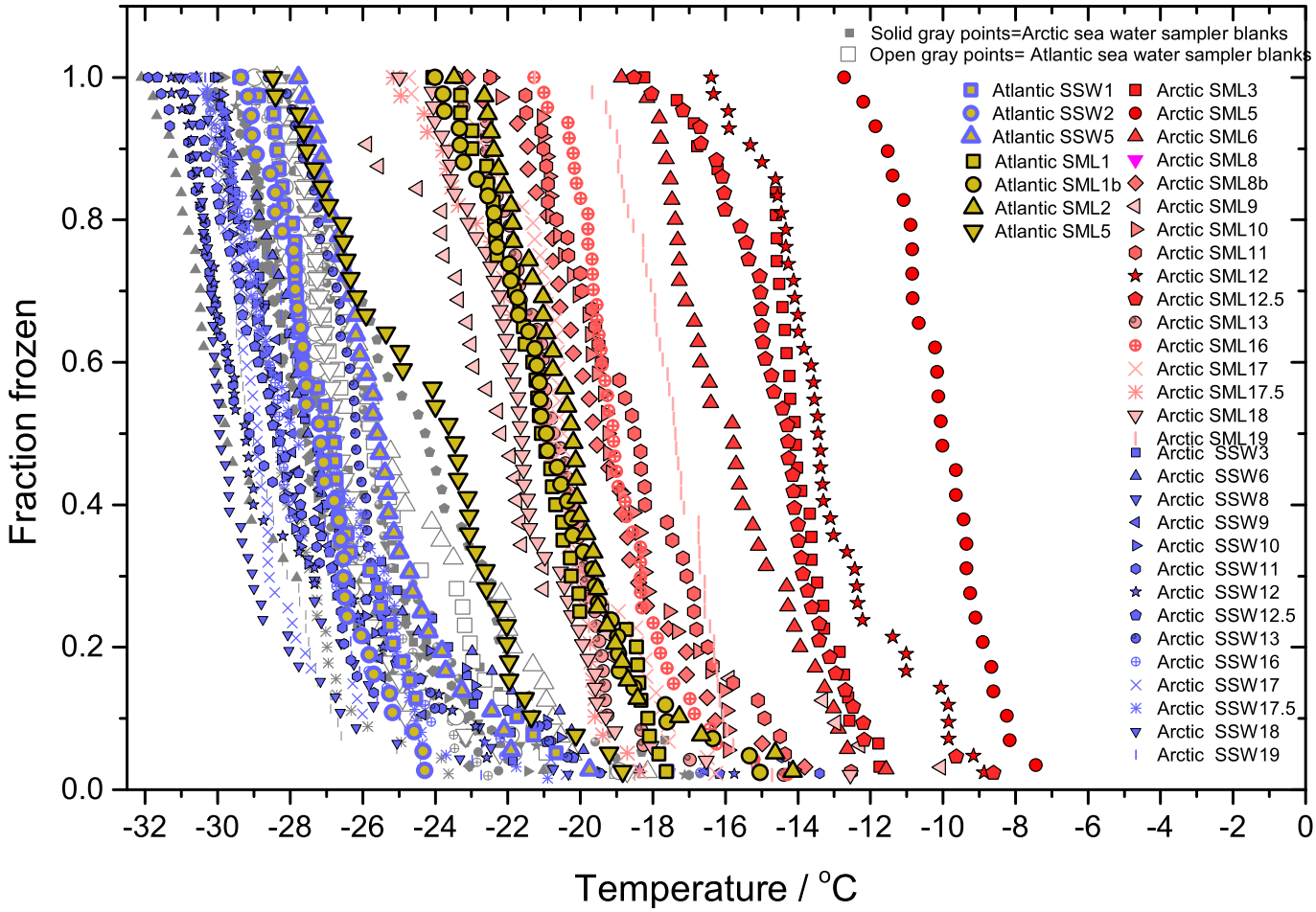

Extended Data Figure 8 | µl-NIPI freezing curves for Arctic and Atlantic samples uncorrected for freezing depression caused by salts. Fraction frozen curves for 1 µl droplet freezing experiments using Arctic and Atlantic ocean samples, uncorrected for freezing point depression. SML, SSW and boat flushing water (grey points; symbols correspond to those for SML sampled at the same locations) to check for the absence of contaminant INPs before sampling.

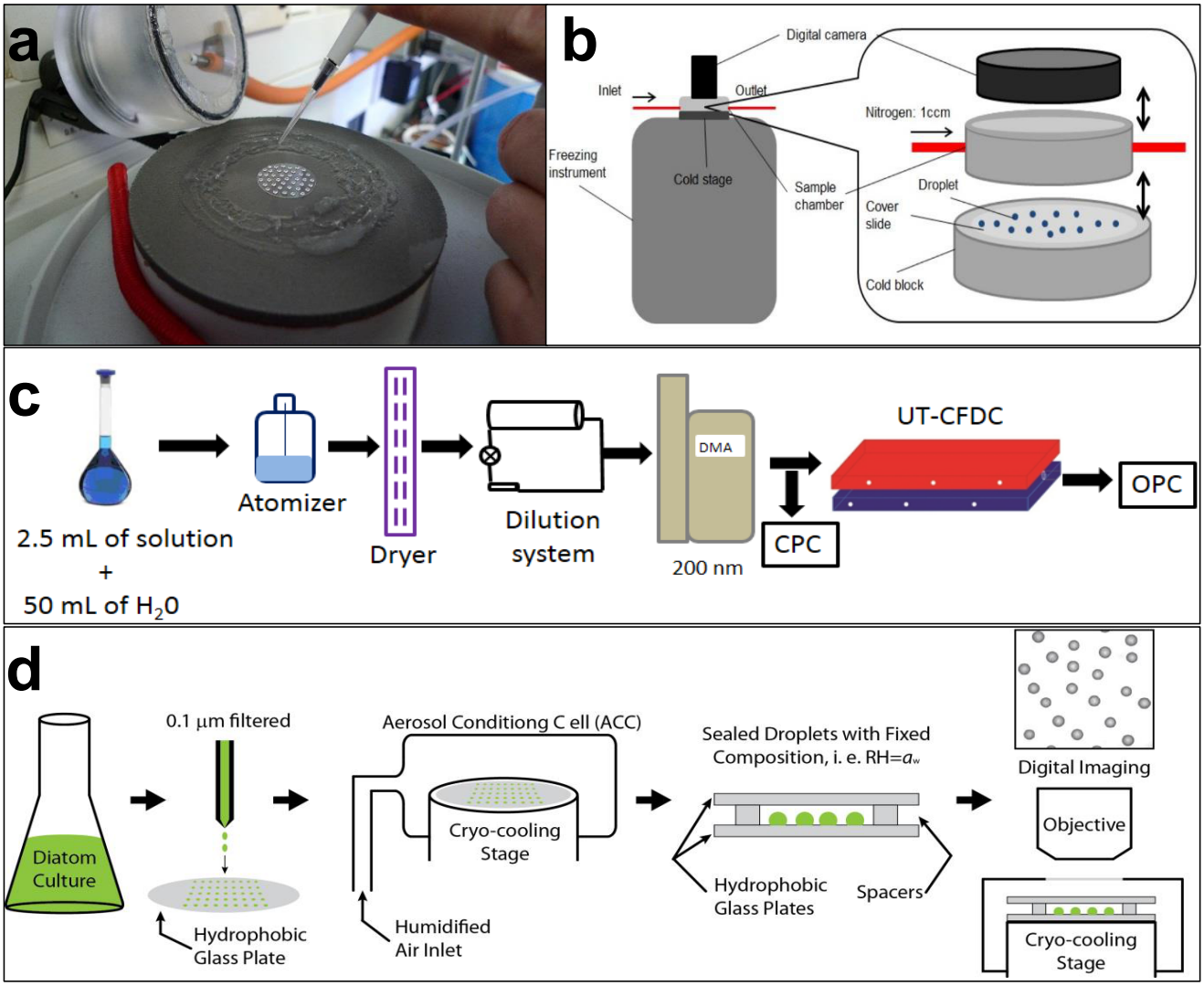

Extended Data Figure 9 | Summary of ice nucleation experimental setups. **a**, Pipetting 1 µl droplets onto a hydrophobic glass slide. **b**, Schematic of the µl-NIPI cold stage used for immersion mode droplet freezing experiments. **c**, Schematic of the experimental setup for cirrus cloud relevant experiments. CPC, condensation particle counter; DMA, differential mobility analyser; OPC, optical particle counter. **d**, Schematic of the water-activity-controlled immersion freezing experiment (WACIFE) for freezing of micrometre-sized droplets containing diatom exudates as a function of water activity, a_w, and relative humidity, RH. Images are not to scale. The procedure for preparing and freezing droplets of filtered and autoclaved natural sea water with and without added f/2 nutrients droplets is similar except 0.1 µm filtration is not required.

Extended Data Table 1 | Details of the sampled SMLs and SSWs

Date	Time / UTC	Location (see Extended data Fig. 1)	Longitude	Latitude	Samples collected	
					SML	SSW/sampling depth
ACCACIA						
19/07/2013	08:22	3	20°41.700W	70°13.494N	Arctic SML3	Arctic SSW3 / 2 m
21/07/2013	07:56	5	20°18.336W	71°53.692N	Arctic SML5	Arctic SSW5 / 5 m
22/07/2013	08:00	6	13°06.120W	73°06.340N	Arctic SML6	Arctic SSW6 / 2 m
24/07/2013	08:02	8	08°43.511W	75°02.956N	Arctic SML8b	Arctic SSW8 / 2 m
25/07/2013	08:07	9	15°31.311W	76°31.902N	Arctic SML9	Arctic SSW9 / 2 m
26/07/2013	14:24	10	5°18.642W	76°16.141N	Arctic SML10	Arctic SSW10 / 2 m
27/07/2013	09:19	11	7°04.645W	77°57.427N	Arctic SML11	Arctic SSW11 / 2 m
28/07/2013	06:15	12	7°01.993W	78°53.663N	Arctic SML12	Arctic SSW12 / 2 m
29/07/2013	08:50	12.5	5°13.61W	77°27.207N	Arctic SML12.5	Arctic SSW12.5 / 2 m
30/07/2013	12:01	13	7°35.043E	74°48.828N	Arctic SML13	Arctic SSW13 / 2 m
03/08/2013	10:20	16	23°56.620E	80°08.900N	Arctic SML16	Arctic SSW16 / 2 m
04/08/2013	07:58	17	33°43.967E	83°18.630N	Arctic SML17	Arctic SSW17 / 0.4 m
04/08/2013	20:48	17.5	33°43.231E	83°18.381N	Arctic SML17.5	Arctic SSW17.5 / 2 m
05/08/2013	07:53	18	26°07.684E	82°41.5N	Arctic SML18	Arctic SSW18 / 2 m
06/08/2013	07:59	19	34°49.928E	81°00.1N	Arctic SML 19	Arctic SSW19 / 0.3 m
WACS II						
23/05/2014	16:13	1	62.3256W	40.41335N	Atlantic SML1	Atlantic SSW1 / 5m
23/05/2014	18:20	1b	62.195878W	40.399563N	Atlantic SML1b	
26/05/2014	18:00	2	61.672607W	42.356586N	Atlantic SML2	Atlantic SSW2 / 5m
04/06/2014	20:30	5	70.5252W	40.68428N	Atlantic SML5	Atlantic SSW5 / 0.5m
NETCARE						
12/08/2013		BC coast	125° 54W	48°93N	BC coast SML1	BC coast SSW1 / 0.5m
12/08/2013		BC coast	125° 54W	48°93N	BC coast SML2	BC coast SSW2 / 0.5m
15/08/2013		BC coast	125°33W	48°54N	BC coast SML3	
15/08/2013		BC coast	125°33W	48°54N	BC coast SML4	
14/06/2013		NE Pacific	138°40.0W	49°34.0N	Pacific SML1	
16/06/2013		NE Pacific	145°00.0W	50°00.0N	Pacific SML2	
16/06/2013		NE Pacific	145°00.0W	50°00.0N	Pacific SML3	Pacific SSW3 / 1 m

Details are given of samples collected during the ACCACIA Arctic cruise, WACS II Atlantic cruise and the NETCARE project. Northeast (NE) Pacific samples were collected as part of the Line P time series, cruise 2013–2017. British Columbia (BC) coast samples were collected in Terrace Bay on the western coast of Vancouver Island (Canada) and at a location approximately 3 km offshore from Ucluelet. Location numbers relate to the maps shown in Extended Data Fig. 1.